From chain growth to step growth polymerization of photo-reactive PCL: the network topology of bioresorbable networks as tool in tissue engineering

*Quinten Thijssen, Laurens Parmentier, Edyta Augustyniak, Pierre-Alexis Mouthuy, Sandra Van Vlierberghe**

Q. Thijssen, L. Parmentier, Prof. Dr. S. Van Vlierberghe
Ghent University, Polymer Chemistry and Biomaterials Group, Centre of Macromolecular Chemistry, Department of Organic and Macromolecular Chemistry, Krijgslaan 281 S4, 9000, Belgium
E-mail: Sandra.VanVlierberghe@ugent.be

Dr. E. Augustyniak, Prof. Dr. PA. Mouthuy
Nuffield department of Orthopaedics Rheumatology and Musculoskeletal Sciences (NDORMS), B4495, Headington, Oxford OX3 7LD, United Kingdom

Keywords: poly(ε-caprolactone), network topology, thiol-ene, thiol-yne, acrylates, digital light processing, tissue engineering

Control of the network topology by selection of an appropriate crosslinking chemistry is introduced as a new strategy to improve the elasticity and toughness of bioresorbable networks. The development of novel photo-crosslinkable and bioresorbable oligomers is essential for the application of light-based 3D-printing techniques in the context of tissue engineering. Although light-based 3D-printing techniques are characterized by an increased resolution and manufacturing speed as compared to extrusion-based 3D-printing, their application remains limited. Via chemical modification, poly-ε-caprolactone (PCL) is functionalized with photo-reactive end groups such as acrylates, alkenes and alkynes. Based on these precursors, networks with different topologies are designed via chain growth polymerization, step growth polymerization or a combination thereof. The influence of the network topology and the concomitant crosslinking chemistry on the thermal, mechanical and biological properties are elucidated together with their applicability in digital light processing. Photo-crosslinkable PCL with an elongation at break of 736.3 % ± 47 % and an ultimate strength of 21.3 MPa ± 0.8 MPa is realized, which is approximately 10-fold higher compared to the current state-of-the-art. Finally, extremely elastic DLP-printed dogbones are developed which can fully retrieve their initial length upon stress relieve at an elongation of 1000 %.

1. Introduction

Bioresorbable synthetic polymers such as poly(ε-caprolactone) (PCL), poly(lactic acid) (PLA) and poly(lactic-co-glycolic acid) (PLGA) have been widely studied in the context of tissue engineering (TE). Despite the fact that they are not cell-interactive, these polymers are interesting candidates for TE due to their biodegradability and mechanical properties combined with excellent biocompatibility. [1–5] Furthermore, their processability via extrusion-based 3D-printing has paved the way towards patient-specific implants (PSI) which have been reported to reduce operation times, operative tissue damage and post-operative infections as a result of the excellent fit with the anatomical structure of the patient.[6–8] However, despite being processable via extrusion-based 3D-printing, without chemical modification, they cannot be processed via light-based additive manufacturing (including laser- and projection-based 3D-printing technologies). Nevertheless, light-based additive manufacturing techniques such as two-photon polymerization (2PP), stereolithography (SLA) and digital light processing (DLP) offer distinct benefits in terms of manufacturing precision and throughput compared to extrusion-based techniques.[9] Yet, despite these advantages, the application of light-based additive manufacturing techniques in the context of TE remains limited due to the lack of photopolymerizable bioresorbable materials with appropriate mechanical properties, as reflected by the limited elongations at break and ultimate strengths of acrylate functionalized polymers which is generally below 100% and 12 MPa, respectively.[9–11]

Within the range of bioresorbable synthetic polymers, PCL has received significant attention due to its FDA approval and relatively slow biodegradation.[12] PCL has been firstly synthesized in 1934 by the Carothers group and is a linear polyester which degrades via the hydrolytic cleavage of the ester bonds resulting in 6-hydroxy caproic acid.[13–15] The relatively long biodegradation time of PCL lowers the effect of local acidification, resulting from the formation of 6-hydroxy caproic acid upon biodegradation. For other polyesters such as PLA and PLGA, as a consequence of their fast biodegradation, this local acidification is considered problematic

due to the inflammatory response it causes.[16] Additionally, PCL can be synthesized starting from relatively cheap monomers with high control. Combined with its superior rheological and viscoelastic properties, it can be considered an ideal polymer for biomedical applications such as drug delivery devices and scaffolds for TE. [12,17,18]

With the aim to render PCL processable via light-based additive manufacturing techniques, recent efforts have focused on the chemical modification of PCL diol in order to obtain its acrylate-functionalized derivative. To date, two distinct derivatization approaches starting from PCL diol have been described, namely via urethane coupling chemistry or via the addition-elimination reaction with acryloyl chloride.[19–21] Nevertheless, as a result of the acrylate crosslinking and the corresponding inhomogeneous network topology, brittle networks are obtained. Non-functionalized, high molar mass PCL is a widely exploited polymer for extrusion-based 3D-printing serving biomedical applications. It is characterized by an elongation at break of 400-900% and an ultimate strength of 12-30 MPa. Acrylate photo-crosslinked PCL, on the other hand, is generally characterized by an elongation at break below 100 % and an ultimate strength below 12 MPa.[22–26] Therefore, despite the fact that bioresorbable photo-crosslinkable PCL has been developed, its biomedical application is lacking due to its inappropriate mechanical properties.

Herein, we introduce control of the network topology as a strategy to optimize the mechanical properties of photo-crosslinked PCL. Indeed, via manipulation of the involved crosslinking chemistry, the network properties can be altered. In pioneering work, Cramer and Bowman illustrated this concept with non-degradable small molecule compounds, by showing that thiol-acrylate systems with different initial stoichiometries exhibit diverse network properties after photopolymerization.[27–29] This effect was attributed to the chain transferring capability of the thiols thereby shifting the chain growth acrylate homopolymerization towards a binary system in which both chain and step growth polymerization are combined. Additionally, step-growth photopolymerizable networks have been developed, based on the thiol-ene/yne reaction,

characterized by high photo-reactivity, reduced oxygen sensitivity and lowered shrinkage.[30–32] Despite the fact that these effects have been documented, they remain unexplored in the context of bioresorbable networks. Therefore, via the functionalization of PCL with photo-reactive groups such as acrylates, alkenes and alkynes, the effect of the different network topologies obtained via chain growth polymerization, step growth polymerization and a combination thereof on the mechanical, thermal and biological properties as well as on the digital light processing printability of photo-crosslinkable PCL is described herein.

2. Results and discussion

2.1. Synthesis of functionalized photo-reactive PCL precursors

In order to render PCL photo-crosslinkable, end-group functionalization with different photo-reactive moieties, namely acrylates, alkenes and alkynes, has been performed via urethane coupling chemistry (**Figure 1**). In a first step, the endcaps with acrylate, alkene and alkyne functionalities were synthesized via the nucleophilic addition reaction of isophorone diisocyanate (IPDI) and 2-hydroxy ethyl, allyl alcohol and propargyl alcohol, respectively. In a second step, PCL diol with a molar mass of 2000 $g.mol^{-1}$, was reacted with the respective endcaps in order to obtain acrylate-, alkene- and alkyne-terminated PCL. These compounds will be further referred to as acrylate-terminated urethane-based polymer (AUP-PCL), ene-terminated urethane-based polymer (EUP-PCL) and yne-terminated urethane-based polymer (YUP-PCL), respectively.

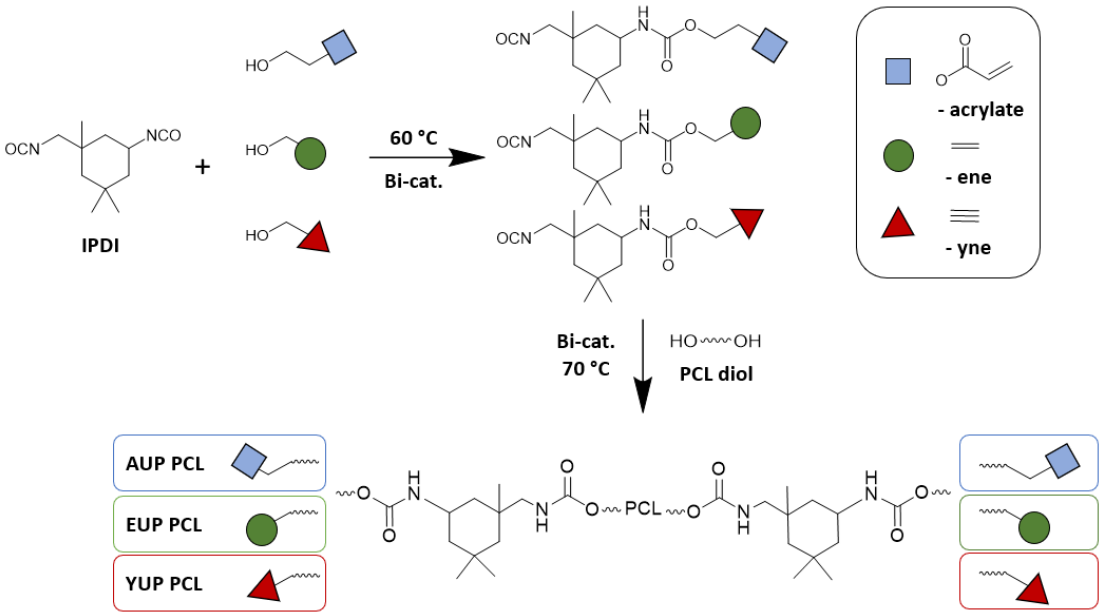

Figure 1. Two-step synthesis protocol of the acrylate- (AUP-PCL), alkene- (EUP-PCL) and alkyne- (YUP-PCL) terminated PCL.

Via quantification of the isocyanate functionalities through the back titration using dibutyl amine, the reaction progress of the first step was monitored. Completion of the second step could be confirmed through FTIR spectroscopy, as the characteristic isocyanate stretching vibration at 2275-2250 cm^{-1} disappeared (illustrated in Figure S1). Successful functionalization with degrees of substitution of 84, 73 and 82% was confirmed for the synthesized acrylate- (AUP-PCL), alkene- (EUP-PCL) and alkyne- (YUP-PCL) functionalized PCL respectively, through quantitative ^{1}H-NMR spectroscopy using dimethyl terephthalate (DMT) as internal standard (Figure 2, S2-S4).

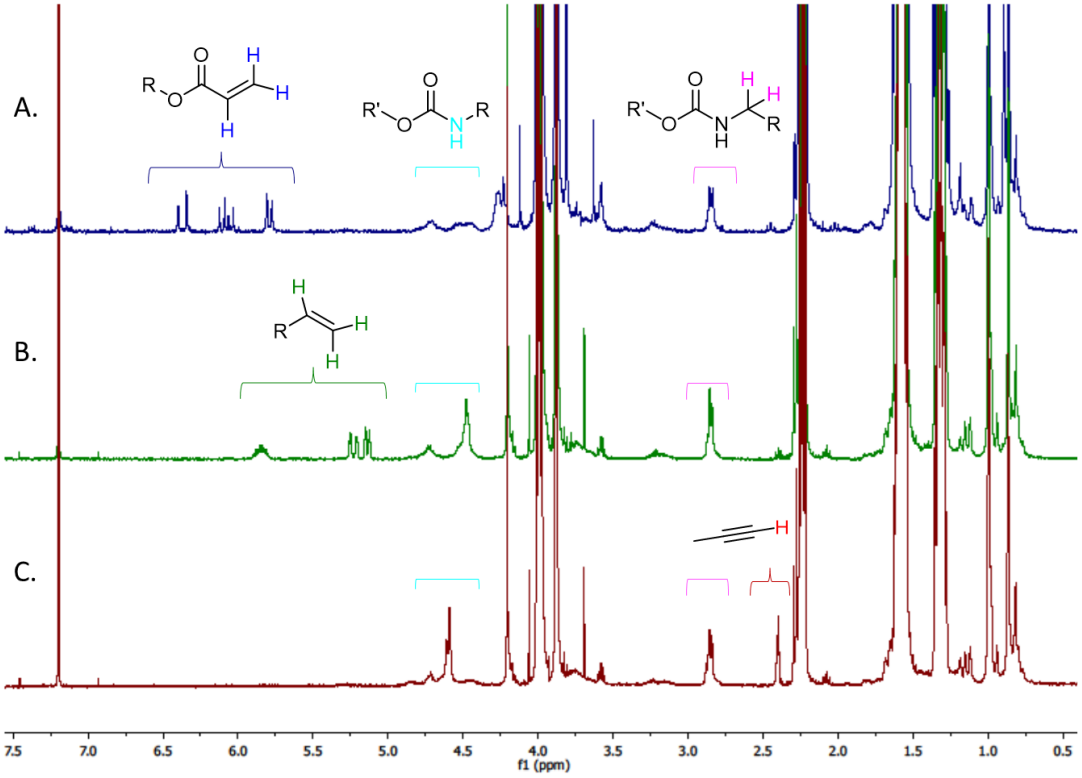

Figure 2. [1]H-NMR spectra of the functionalized PCLs with A. acrylates (AUP-PCL); B. enes (EUP-PCL); C. ynes (YUP-PCL) in presence of DMT.

2.2. Design of different network topologies

Based on the synthesized oligomeric precursors, four networks with different network topologies were prepared as a result of the chemistries involved (Figure 3). In order to photo-crosslink the respective networks, 2 mol.% ethyl (2,4,6-trimethylbenzoyl) phenylphosphinate (TPO-L, with respect to the amount of terminal functionalities) has been incorporated prior to UV-A irradiation (10 mW/cm²). A first network was prepared via crosslinking of AUP-PCL, without an additional crosslinker, resulting in purely chain growth polymerization of the acrylate functionalities (Figure 3A). In order to shift the chain growth polymerization to a binary system in which both step and chain growth polymerization are combined, AUP-PCL has been combined with (pentaerythritol tetrakis(3-mercaptopropionate)) (PETA-4SH) (i.e. AUP-PCL + PETA-4SH). PETA-4SH is a tetrafunctional thiol which can act as a chain transfer agent, thereby shifting the polymerization from purely chain growth to a combination of both step and chain growth polymerization (Figure 3B). Whether the polymerization will occur via

a chain or step growth mechanism depends on whether the ene moiety is able to undergo radical homopolymerization. Enes such as allyl ethers, vinyl ethers and norbornenes do not homopolymerize, while acrylates and methacrylates do.[32] Furthermore, the extent of step or chain growth depends on the ratio of the kinetic rate constants for the propagation and chain transfer reactions.[30] In order to combine both step and chain growth polymerization, an acrylate to thiol ratio of 2:1 was selected. Since the ratio of the thiol propagation to the homopolymerization rate constant is close to 8, the thiyl radical will react much faster with an acrylate compared to the acrylate homopolymerization itself.[33] Furthermore, a complete step growth polymerized network was designed via the combination of EUP-PCL and PETA-4SH (Figure 3C). Based on the orthogonality of the thiol-ene reaction, an alkene to thiol ratio of 1:1 was selected. Finally, a fourth network was prepared via the thiol-yne reaction through the combination of YUP-PCL and PETA-4SH (Figure 3D). Similar to the thiol-ene network, the polymerization occurs via a step growth mechanism. However, since an alkyne functional group subsequently reacts with two thiol functionalities, the crosslinking density will be twice that of the thiol-ene based network (i.e. EUP-PCL+ PETA-4SH).[34] Therefore, an alkyne to thiol ratio of 1:2 was selected for the preparation of the thiol-yne network (i.e. YUP-PCL + PETA-4SH).

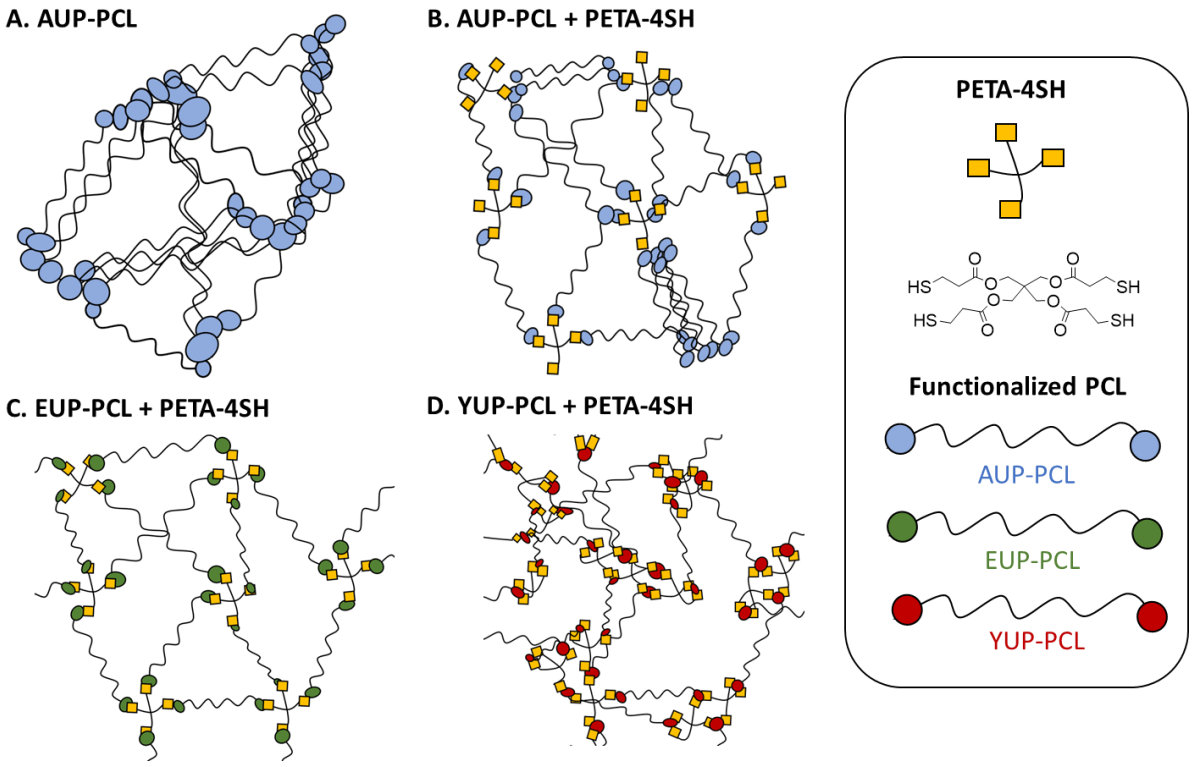

Figure 3. Schematic representation of the different topologies of the photo-crosslinked PCL networks, stemming from the involved crosslinking chemistries; A. Acrylate crosslinking (AUP-PCL); B. Acrylate-thiol crosslinking (AUP-PCL + PETA-4SH); C. Thiol-ene crosslinking (EUP-PCL + PETA-4SH); D. Thiol-yne crosslinking (YUP-PCL + PETA-4SH).

2.3. Network integrity and photo-reactivity

In order to investigate the network integrity, gel fraction and swelling experiments have been performed (Table 1). Gel fractions exceeding 80 % have been retrieved for all networks indicating good network integrity and successful network formation. As swelling experiments hold information about the network topology and crosslink density, they can give a valuable first impression of the influence of the different crosslinking chemistries.[35,36] The lowest swelling ratio of 6.2 ± 0.1 was retrieved for the thiol-yne crosslinked network (YUP-PCL + PETA-4SH). This could be expected based on the fact that one alkyne functionality will react with two thiol functionalities, thereby leading to an increased crosslink density. It can be hypothesized that this increased crosslink density leads to the formation of a more rigid network and therefore reduces the swelling capacity. Furthermore, swelling ratios for the acrylate-containing networks of 7.2 ± 0.1 (AUP-PCL) and 12.7 ± 0.2 (AUP-PCL + PETA-4SH) were

determined without and with the addition of the tetrafunctional thiol (PETA-4SH), respectively. These results reveal that the incorporation of the tetrafunctional thiol (PETA-4SH) leads to an increased swelling capacity of the networks. This effect can be attributed to the more homogeneous network topology that is obtained via the combination of chain and step growth polymerization as a result of the introduced thiol.[37] Furthermore, a swelling ratio of 10.6 ± 0.1 was retrieved for the thiol-ene photo-crosslinked PCL (EUP-PCL + PETA-4SH). Also here, an increase in the swelling ratio, compared to the purely acrylate photo-crosslinked PCL (AUP-PCL), was found. This effect can also be attributed to the more homogeneous network topology that is obtained via thiol-ene crosslinking.[37] Finally, in order to determine whether quantitative conversion of the photo-reactive groups had taken place, the networks were evaluated through high resolution magic angle spinning (HR-MAS) ^{1}H-NMR spectroscopy (Figure S5). HR-MAS ^{1}H-NMR spectroscopy allows to elucidate the chemical composition of crosslinked samples and can therefore be used to investigate the fraction of residual functional groups post-crosslinking. Quantitative conversion of the photo-reactive moieties is of utmost importance since remaining unreacted functional groups, such as acrylates can be cytotoxic and can cause foreign body responses leading to inflammation.[38] However, evaluation of the characteristic peaks corresponding to the acrylate, alkene and alkyne functionalities indicated quantitative conversion.

Table 1. Gel fractions, swelling ratios and substitution degrees obtained for the different photo-crosslinked PCL networks.

	Gel fraction (%) [a]	Swelling ratio [a]	Substitution degree (%)
AUP-PCL	92.2 ± 0.7	7.2 ± 0.1	73
AUP-PCL + PETA-4SH	88.4 ± 1.3	12.7 ± 0.2	73
EUP-PCL + PETA-4SH	80.9 ± 2.2	10.6 ± 0.1	63
YUP-PCL + PETA-4SH	86.8 ± 0.6	6.2 ± 0.1	80

a) all experiments have been performed in $CHCl_3$

Furthermore, the photo-reactivity of the oligomeric precursors is of utmost importance since it will influence the polymerization kinetics and can affect the ability to process the materials via

light-based 3D-printing techniques (including laser- and projection-based systems) such as two-photon-polymerization (2PP), stereolithography (SLA) and digital light processing (DLP). For example, oligomers with high photo-reactivity can be crosslinked using shorter irradiation times and lower light intensities. This will consequently reduce the manufacturing time and improve the cost-efficiency and resolution of the technique.

Via photo-rheology, the influence of the crosslinking chemistries on the photo-crosslinking kinetics of the photo-crosslinked PCLs has been investigated (Figure 5A). The gel point (i.e. crossover of the G' and G'') of the various networks were determined to be 2.5, 4.8, 4.8 and 717 seconds for the acrylate, acrylate-thiol, thiol-ene and thiol-yne crosslinked PCL, respectively. The significantly slower photo-crosslinking of the thiol-yne system is in agreement with literature, since it has been reported that thiols react significantly faster with allyl ethers and acrylates compared to alkynes.[30,32,39] Additionally, we see that thiol incorporation results in a delayed gelation. This can also be expected due to the shift towards a step growth polymerization mechanism which is assumed to result in a delayed increment of the molar mass. Furthermore, it can be seen that the final storage modulus (G'), obtained after photo-crosslinking, depends on the involved crosslinking chemistry. Post polymerization storage moduli of 0.4, 0.3, 0.1 and 0.006 MPa were determined for the acrylate, acrylate-thiol, thiol-ene and thiol-yne photo-crosslinked PCL, respectively. Also here, a reduction in post-polymerization storage modulus can be seen upon introduction of the thiols, which can be attributed to the step growth polymerization mechanism as well. In literature it is described that the delayed gelation lowers the stress accumulated during photo-polymerization. The significantly lower post-polymerization storage moduli for the thiol-yne photo-crosslinked PCL is hypothesized to result from an incomplete photo-crosslinking. More specifically, due to the slow photo-crosslinking kinetics, the plateau value was not yet reached after the end of the photo-rheology experiment (i.e. 1000 seconds). It should be noted that the reduced photo-reactivity was taken into account during photo-crosslinking of the samples for further

characterization (i.e. irradiation for 2 hours instead of 30 minutes was performed). Complete photo-crosslinking was confirmed via HR-MAS ^{1}H-NMR spectroscopy as well as a high gel fraction (> 87 %). Hence, incomplete photo-crosslinking is not expected to influence further characterization. However, due to the slow photo-crosslinking kinetics characteristic for thiol-yne photo-crosslinking, these materials are considered unusable in the context of light-based 3D-printing. It should be noted that the values for the storage modulus (G') obtained via photo-rheology, are prior to crystallization, and thus, are not representative for the effective mechanical properties of the respective materials. Overall, it can be concluded that, except for the thiol-yne photo-crosslinked PCL, all networks exhibited excellent photo-reactivity and crosslinking kinetics leading to complete crosslinking within a range of several seconds.

2.4. Thermal properties

Thermogravimetric analysis (TGA) and differential scanning calorimetry (DSC) were employed to investigate the influence of the network topology on the thermal properties (Table 2).

Table 2. Thermal properties of the different photo-crosslinked PCL networks.

	T_g (°C) [b]	T_d (°C)	T_c (°C) [b]	ΔH_c (J/g) [b]	T_m (°C) [b]	ΔH_m (J/g) [b]	X (%)
AUP-PCL	-59.9 ± 0.5	366	-17.9 ± 1.2	3.6 ± 0.6	35.4 ± 0.2	37.3 ± 0.3	28
AUP-PCL + PETA-4SH	-55.5 ± 0.3	366	-15.4 ± 0.4	4.9 ± 0.4	38.5 ± 0.1	40.8 ± 0.6	30
EUP-PCL + PETA-4SH	-53.8 ± 0.2	358	-15.7 ± 0.3	9.1 ± 1.0	40.0 ± 0	37.8 ± 0.7	28
YUP-PCL + PETA-4SH	-52.6 ± 1.8	355	ND [a]	ND [a]	39.4 ± 0.2	1.4 ± 0.2	1
PCL 70 000 – 90 000	-64.1	374	20.6	56.2	55.2	61.7	46

[a] ND = not detected. [b] reported values are the average ± standard deviation (N = 3).

Degradation temperatures (determined at the onset) of 366, 366, 358 and 355 °C were determined for the acrylate (AUP), acrylate-thiol (AUP + PETA-4SH), thiol-ene (EUP + PETA-4SH) and thiol-yne (YUP + PETA 4S) photo-crosslinked PCL, respectively. Non-functionalized, high molar mass PCL is ubiquitous in tissue engineering and can be considered the gold standard with respect to extrusion-based 3D-printing for tissue engineering purposes. Therefore, throughout the study, PCL with a molar mass of 70 000 – 90 000 g.mol^{-1} was

included as benchmark. As can be seen in Table 2, the degradation temperatures obtained for the photo-crosslinked PCLs correspond well with the benchmark material. Furthermore, these results are in line with previously reported values for PCL.[12] Thus, the thermal stability was not affected by the different types of crosslinks that were introduced. In the context of their application, it can be stated that all networks have excellent temperature stability. Additionally, glass transition temperatures of – 60, - 56, -54 and – 53 °C were retrieved for the acrylate (AUP-PCL), acrylate-thiol (AUP + PETA-4SH), thiol-ene (EUP + PETA-4SH) and thiol-yne (YUP + PETA-4SH) based networks, respectively. Again, these values are in good agreement with the benchmark as well as with earlier reported values for linear PCL.[12] Although appropriate network formation has been confirmed, after photo-crosslinking, all networks retain sufficient chain mobility to allow for melting and recrystallization. Upon further investigation of the melting and crystallization behavior for the various networks, a surprising finding was observed. After storing of the samples at room temperature, two melting peaks were observed instead of one. More specifically, in the second heating cycle (after erasing the thermal history of the networks) a single melting peak (Figure 4A). However, when the materials were stored at room temperature, the melting enthalpy changed and two distinct melting peaks were retrieved (Figure 4B). It is hypothesized that this behavior can be attributed to phase separation phenomena, able to occur at room temperature, thereby forming urethane- and PCL- rich segments. The crystallinity in the first heating cycle (i.e. after storing the materials at room temperature) was significantly higher in case of the more homogeneous network topology. Based on this observation, it is hypothesized that the more homogeneous network topology (i.e. thiol-ene photo-crosslinked PCL) enables the phase-separation to a higher extent, without resulting in a reduction of the melting enthalpy. Conversely, the acrylate photo-crosslinked PCL, shows a significant reduction in initial melting enthalpy of ~13.2 $J.g^{-1}$ after being stored at room temperature. It can be anticipated that its inhomogeneous network topology does not allow phase separation without reduction of the melting enthalpy. As the acrylate-thiol photo-

crosslinked PCL (AUP-PCL + PETA-4SH) is formed via a combination of both chain and step growth polymerization, it can be anticipated that the observed behavior would be a combination of both above-described behaviors. As can be seen in Figure 4B, this is indeed the case, revealing a melting enthalpy reduction of ~ 11.2 $J.g^{-1}$. Although for the thiol-yne photo-crosslinked PCL (YUP-PCL + PETA-4SH) crystallization was not observed within the timeframe of the performed DSC experiments, it was observed that after storing the sample for several days, this network crystallized as well. It is assumed that the slower crystallization kinetics are due to the more densely photo-crosslinked network. Furthermore, no formation of a second melting peak could be observed, indicating that the highly rigid network (i.e. increased crosslink density) might prevent the hypothesized phase-separation from occurring. However, the proposed assumptions should be approached with caution as further confirmatory studies may be appropriate. Furthermore, the crystallinity (based on the melting enthalpy of the 2^{nd} heating cycle) of all networks ranged between 26 and 30 %, except for the thiol-yne photo-crosslinked PCL. However, after storing this materials for one week, a crystallinity of 25 % was measured. This illustrates that, although slower, this network crystallized to a similar extent compared to the other photo-crosslinked networks. Finally, if the crystallinity of the photo-crosslinked PCLs is compared to that of the benchmark (PCL 70 000 – 90 000 $g.mol^{-1}$), a significantly higher crystallinity for the benchmark was found (46 vs 30 %). This effect can be attributed to the absence of the urethane segments in case of the reference material.

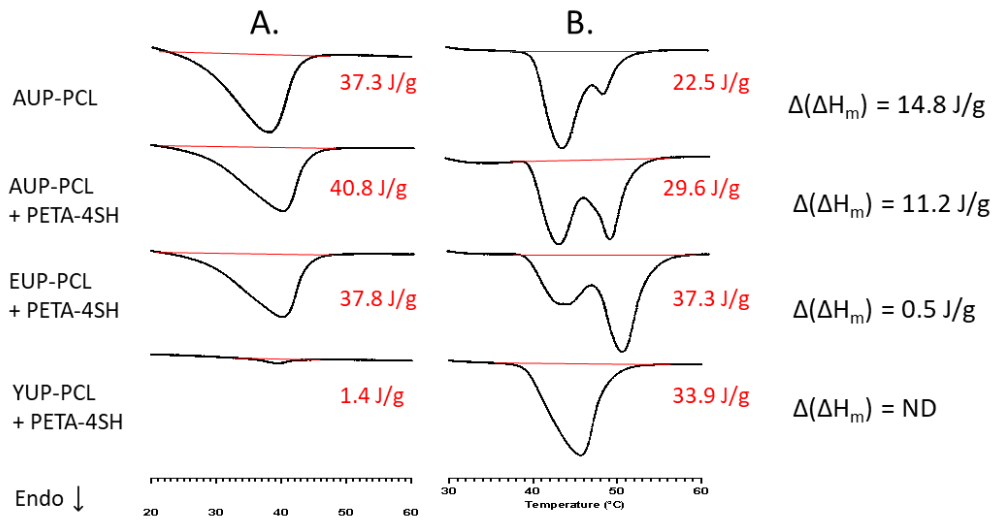

Figure 4. DSC thermograms of the different photo-crosslinked PCL networks A. During the second heating run (after erasing the thermal history); B. During the first heating run – after storing the sample at room temperature during one week. The difference in enthalpy of fusion is indicated for each sample, except for the thiol-yne based network (ND = not determined).

Additionally, the thermal/mechanical transitions of the networks were analyzed via dynamic mechanical analysis (DMA) (Figure S6). As anticipated, from approximately – 50°C, once the glass transition temperature is reached, the storage moduli start to gradually decrease. The onset of this decrease is slightly shifted to higher temperatures for the more homogeneous networks, as a result of the slightly increased glass transition temperatures. This also indicates a more narrow transition, and thus, a more uniform network topology. In order to verify this, the tan δ values of the networks are plotted in Figure 5B. Based on the tan δ, the full width at half maximums (FWHM) were determined. The broadness, characterized by the FWHM of the tan δ, is reported in literature as a measure for the homogeneity of a network.[37,40] FWHM values of 105, 60, 63 and 74 °C were determined for the acrylate (AUP-PCL), acrylate-thiol (AUP-PCL + PETA-4SH), thiol-ene (EUP-PCL + PETA-4SH) and thiol-yne (YUP-PCL + PETA-4SH) photo-crosslinked PCL, respectively. Compared to the purely acrylate photo-crosslinked PCL, all networks show a reduction in the FWHM, thereby confirming the more homogeneous network topology anticipated based on the network design (chain growth polymerization, step growth polymerization and a combination thereof). However, it should be noted that similar

FWHMs for the acrylate-thiol and the thiol-ene crosslinked network were retrieved, which would indicate similar homogeneity for the respective networks. Furthermore, the DMA analysis shows that when the melting temperature is reached, at approximately 40-45 °C, the storage moduli decrease as a result of the loss of the crystallinities of the networks, which is also in agreement with the values obtained via DSC.

2.5. Mechanical properties

Fine-tuned mechanical properties are of utmost importance in tissue engineering in order to provide sufficient mechanical support and to prevent stress-shielding. For example, if a scaffold is stronger than native tissue, it will prevent the surrounding tissue from being mechanically loaded. This can influence the healthy homeostatic balance of the cells and lead to deterioration of the tissue (so-called stress-shielding).[41] Furthermore, it is known that the modulus of a material can influence the behavior of cells including proliferation and differentiation towards certain lineages.[42]

Therefore, via tensile testing of dog bone-shaped test specimens (20 mm gauge length, 0.5 mm gauge thickness, 4 mm gauge width), the Young's modulus, ultimate strength, elongation at break and the toughness of the different networks were determined (Table 3). In order to foster comparison with non-functionalized, high molar mass PCL, the benchmark (PCL 70 000 – 90 000 $g.mol^{-1}$) was included for tensile testing as well. The obtained results reveal that the different network topologies (i.e. photo-crosslinking chemistries) have an unprecedented effect on the mechanical properties of the photo-crosslinked PCLs. It can be observed that networks with a more homogeneous network topology (thiol-acrylate, thiol-ene and thiol-yne) exhibited an increased Young's modulus, compared to the acrylate-crosslinked network. It is hypothesized that the Young's modulus is mainly governed by the crystallinity of the materials. This assumption is supported by the analysis of a non-crystallized dog-bone of AUP-PCL (tested directly after crosslinking, prior to crystallization) which exhibited a Young's modulus of only 4 MPa. This is significantly lower compared to the value obtained in the crystalline state

(38.7 ± 4.1 MPa). The hypothesis is further supported by the excellent agreement between the trend in the Young's moduli and the melting enthalpies (and crystallinity) obtained after storage at room temperature (*vide supra*). Additionally, PCL 70 000 – 90 000 g.mol^{-1} has a crystallinity and Young's modulus which is approximately 2-fold higher compared to thiol-ene crosslinked PCL, supporting the hypothesis as well. The crystallinity of the materials thus seems to be influenced by the network topology. In the context of tissue engineering, this can be an interesting feature since it could be used as a tool to fine-tune the mechanical properties to mimic a specific tissue type. Looking at the elongation at break and the ultimate strength, a similar trend can be observed (Figure 5C). More specifically, except for the thiol-yne network, the more homogeneous the network topology, the higher the elongation at break and consequently, the higher the ultimate strength. It should be noted that this effect is very well reflected in case of the thiol-ene photo-crosslinked PCL (EUP-PCL + PETA-4SH), which theoretically is a perfectly homogeneous network. As a result, an ultimate strength of 21.3 ± MPa and an elongation at break of 736.3 ± 47 were found, which are a multi-fold greater compared to acrylate-terminated PCLs, reported in the state-of-the-art covering photo-crosslinkable PCL.[19–21,43] If the photo-crosslinked PCLs are compared with the benchmark material (PCL 70 000 – 90 000 g.mol^{-1}), several observations can be made. First, the difference in crystallinity results in a significant difference of the Young's moduli (221 vs 93 MPa). However, it is assumed that increasing the molar mass of the oligomer precursors would result in an increase of the Young's modulus resulting from an increased crystallinity. This would be an interesting aspect for future research as it would improve the resemblance between photo-crosslinked PCL and high molar mass PCL. Second, the elongation at break of the benchmark PCL remains higher compared to the photo-crosslinked PCLs. However, in case of the thiol-ene photo-crosslinked PCL, the difference is non-significant ($p = 0.1116$). These results suggest that the elongation at break of thiol-ene photo-crosslinked PCL is comparable to that of linear PCL with a molar mass of 70 000 – 90 000 g.mol^{-1}, which is widely reported in the context of

extrusion-based 3D-printing for biomedical applications, but which cannot be applied in light-based 3D-printing techniques.[22] Consequently, this material has the potential to pave the way towards the use of light-based 3D-printed PCL for biomedical applications. It is hypothesized that the unprecedented, excellent mechanical properties are the result of a synergetic effect of the crystallinity of the material, the presence of hydrogen bonding as a result of the urethane segments and the homogeneous network topology obtained via thiol-ene photo-crosslinking. Finally, it can be observed that, in case of the thiol-yne photo-crosslinked PCL (YUP-PCL + PETA-4SH), the elongation at break (36 ± 17%) and ultimate strength (4.1 ± MPa) are significantly lower. It is assumed that this is due to the increased crosslink density. In turn, this is expected to introduce more rigidity into the network. Therefore, although counter-intuitive, a higher crosslink density does not necessarily imply superior mechanical properties. Especially in a biomedical context, where materials should be easy to handle by the surgeon without fracturing, brittle networks obtained via an increased crosslink density are clearly not beneficial. Finally, these effects are very well reflected in the toughness of the different materials. The increased elongation at break and ultimate strength, drastically improve the toughness of the networks. The thiol-ene photo-crosslinked network exhibits a toughness which is a 10-fold higher compared to that of the acrylate crosslinked network, further highlighting the application potential for this type of network for biomedical applications.

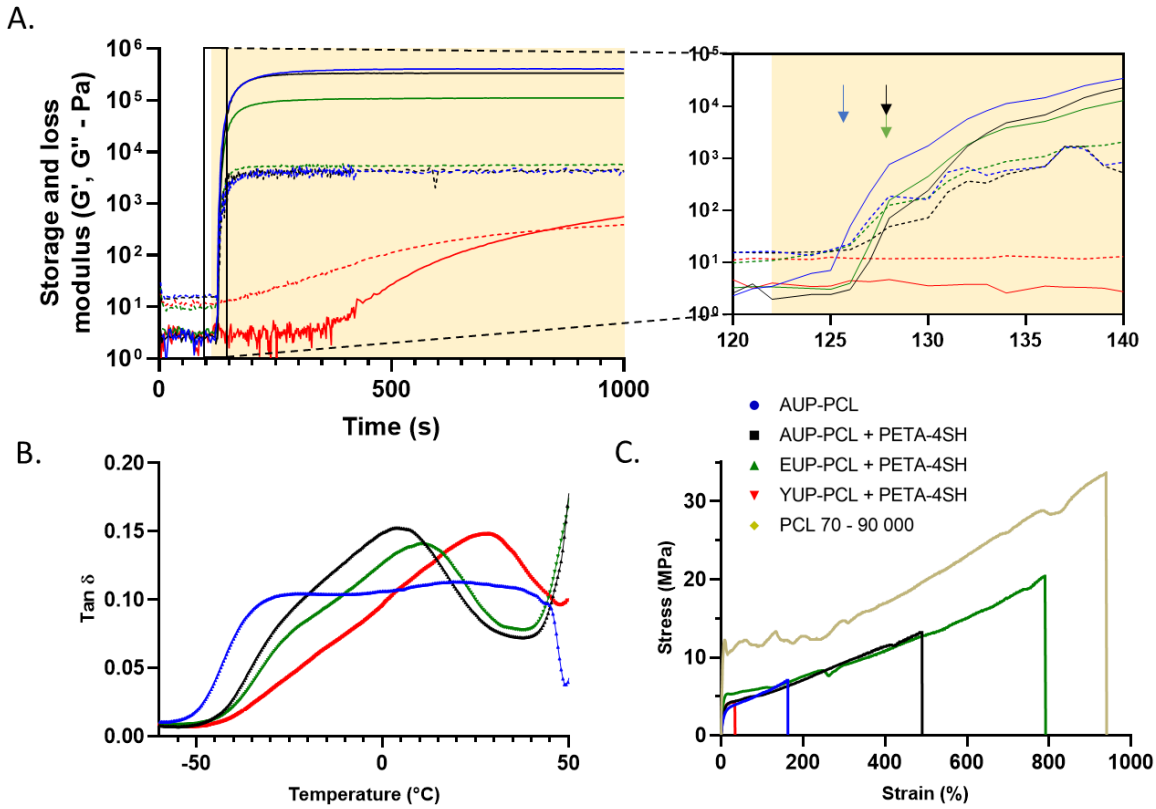

Figure 5. A. Photo-crosslinking kinetics evaluated by photo-rheology upon UVA irradiation (10 mW/cm²). Storage and loss moduli are represented by a solid and dashed line, respectively. On the right, the initial increment of the moduli is illustrated in a zoom and the respective gelation points are indicated with arrows; B. Tan δ of the materials determined via DMA; C. Mechanical properties illustrated by the stress-strain curves obtained through tensile testing. Legend is included in the graph.

Table 3. Young's moduli, elongations at break, ultimate strengths and toughness's obtained via tensile testing of the different photo-crosslinked PCL networks.

	Young's modulus (MPa)	Elongation at break (%)	Ultimate strength (MPa)	Toughness (MJ.m^{-3})
AUP-PCL	38.7 ± 4.1	177 ± 45	7.5 ± 1.6	886 ± 345
AUP-PCL + PETA-4SH	50.6 ± 2.3	514 ± 104	13.6 ± 2.2	4329 ± 1416
EUP-PCL + PETA-4SH	93.4 ± 5.3	736 ± 47	21.3 ± 0.8	8660 ± 245
YUP-PCL + PETA-4SH	70.5 ± 4.0	36 ± 17	4.1 ± 0.3	130 ± 76
PCL 70 000 – 90 000 g.mol^{-1}	221.2 ± 22.7	924 ± 153	32.3 ± 3.9	17939 ± 4443

[a)] reported values are the average of triplicates ± standard deviation (N = 3).

2.6. Indirect cytotoxicity testing

One of the major prerequisites for successful and safe use of a biomedical implant is its biocompatibility. Preclinical evaluation of medical device biocompatibility includes extensive

in vitro and *in vivo* testing, with estimation of cytotoxicity being one of the fundamental steps. Here, we used an in-house Neutral Red Uptake (NRU) cytotoxicity test, guided by the ISO 10993-5:2009 standard, as an indirect cytotoxicity test recommended as part of the biological evaluation of medical devices. The NRU assay is based on the ability of viable cells to incorporate and bind the supravital dye neutral red in lysosomes and provides a quantitative estimation of the number of viable cells in a cell culture.

Cytotoxicity of the photo-crosslinked PCLs was tested in the *in vitro* system, using 3T3 mouse fibroblast cell line, exposed to test compounds over a range of concentrations (Figure 6A). After 24 h exposure, NRU was determined for each treatment concentration and compared to that of control culture. The results of the 3T3 NRU cytotoxicity test confirmed non-cytotoxicity of materials, with relative cell viability for the highest concentration of the sample extract (100% extract) being ≥ 70 % of the control group, as required by ISO-10993-5.

Further increasing the relevance of the *in vitro* biocompatibility testing set-up, primary human foreskin fibroblasts (HFFs) were used in direct contact with the developed materials and evaluation occurred 7 days after contact induction in terms of biocompatibility according to the ISO-10993-5:2009 standard. Again, non-functionalized, high molar mass PCL (70 000 – 90 000 $g.mol^{-1}$) was included as benchmark. The viability of the seeded cells was evaluated through a Live/Dead assay up to 7 days. The red fluorescent dye propidium iodide is taken up in the cell nucleus after a loss in membrane integrity through cell death. Calcein acetoxymethyl, on the other hand, is incorporated by living cells and is converted into its green-fluorescent adduct calcein via intracellular esterases. All samples showed high viabilities both quantitatively (Figure 6B) and qualitatively (Figure 6D). Compared to the benchmark, the differences between the obtained viabilities were non-significant. Furthermore, no significant difference was observed between the photo-crosslinked PCLs compared to the monolayer of fibroblast cells seeded onto tissue culture plate (TCP) and cell viabilities were highly above the minimum requirement of 70 % according to the ISO-standard (10993-5:2009).

Furthermore, the metabolic activity of the HFFs was evaluated via an MTS assay after 7 days upon direct contact with the photo-crosslinked PCLs. Here, the tetrazolium salt is reduced by NAD(P)H-dependent dehydrogenase enzymes in viable cells which acts as a direct marker of cellular metabolic activity. As shown in Figure 6C, the metabolic activity of the HFFs after 7 days in direct contact with the materials (and the benchmark) differs less than 2 % compared to TCP.

In the past, comprehensive *in vitro* and *in vivo* tests have been carried out to demonstrate the safety of PCL, which under the requirements of ISO-10993 has been declared non-toxic and fully biocompatible.[12] The NRU, Live/Dead and MTS biocompatibility results presented here suggest that incorporation of relatively small amounts of photo-crosslinkable moieties (i.e. acrylates, alkenes, alkynes and thiols) did not affect the toxicity of the different photo-crosslinked PCL networks.

Additionally, the differentiation induction potential of the benchmark and different photo-crosslinked PCLs was evaluated. To do so, a thin gelatin coating (± 1 µm) was applied onto the different materials using a previously established dip-coating approach.[44] Adipose derived stem cells (ADSCs) were then seeded onto the photo-crosslinked PCLs and cultured under osteogenic conditions. After 14 days, the presence of Ca^{2+}-depositions was observed via Alizarine red staining of the materials, both qualitatively (Figure 6E) and quantitatively (Figure 6F). As illustrated in Figure 6E, Ca^{2+}-deposits were present on all materials. These findings are in line with previously reported results for non-functionalized PCL.[45,46] Interestingly, quantification of the Ca^{2+}-deposits shows that the osteogenic induction potential of the different photo-crosslinked PCLs differs. The highest osteogenic induction potential was found for non-functionalized, high molar mass PCL (PCL 70 – 90 000 $g.mol^{-1}$). Mooney and co-workers have reported that the mechanical properties of a material can significantly affect the differentiation potential of stem cells.[47] Therefore, it is hypothesized that the difference observed herein can be attributed to the significantly higher Young's modulus of the benchmark material compared

to the other materials. Furthermore, for the photo-crosslinked PCLs, a correlation exists between the metabolic activity determined via the MTS assay and the observed Ca^{2+}-concentrations. Based on this, it is assumed that an increased metabolic activity of the cells (i.e. increased cell proliferation) might result in an increased amount of cells. In turn, this might attribute to the observed differences in Ca-concentration. Overall, these results further indicate that no cytotoxicity is concomitant with the introduction of relatively small amounts of photo-reactive moieties (acrylates, alkenes, alkynes and thiols) in order to photo-crosslink PCL.

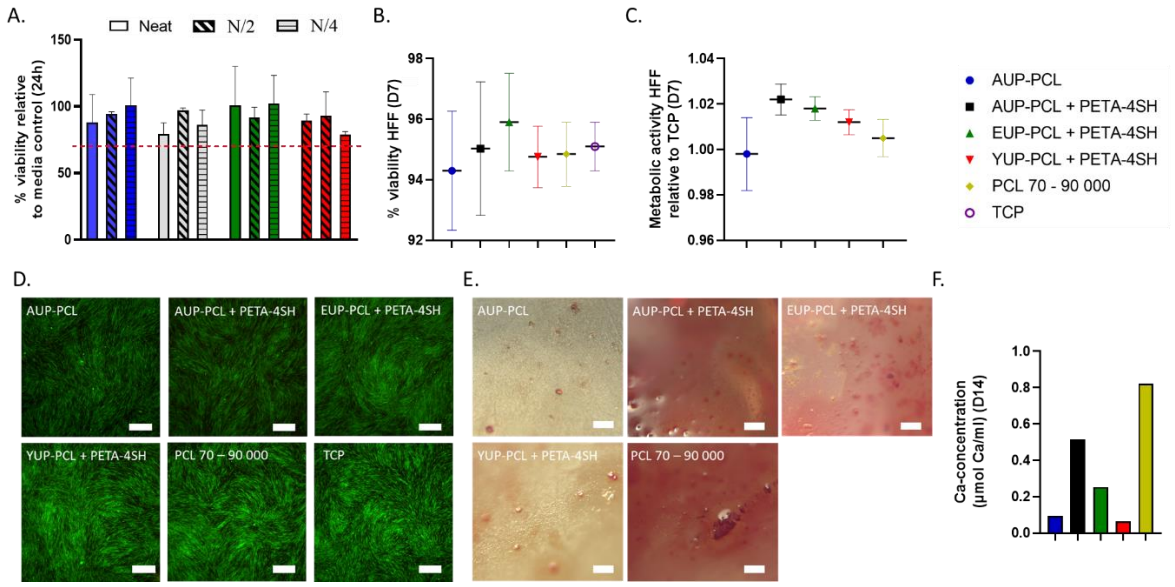

Figure 6. A. Indirect cytotoxicity assay (Neutral red uptake) on material extracts after 24 hours exploiting a 3T3 cell line. N represents undiluted extract. N/2 and N/4 represent 2-fold and 4-fold dilutions of N, respectively; B. Live/dead ratio (Calcein acetoxymethyl/Propidium iodine) showing high viability of HFFs (human foreskin fibroblasts) after 7 days in direct contact with photo-crosslinked samples; C. Metabolic activity assay (MTS) of HFFs after 7 days in direct contact revealing similar metabolic activity as compared to cells seeded onto TCP; D. Live/dead staining illustrating viable and healthy HFFs after 7 days in direct contact with photo-crosslinked samples. Scale bars represent 250 µm; E. Alizarine-red staining showing Ca-deposits after 14 days of culturing ADSCs on gelatin-coated samples. Scale bars represent 100 µm; F. Ca-concentration determined via Alizarine-red staining after 14 days of culturing ADSCs (adipose derived stem cells) on gelatin-coated samples. Legend is included in the graph.

2.7. Digital light processing (DLP)

Based on the photo-reactivity of the developed materials, it can be anticipated that they could make excellent candidates for light-based 3D-printing. Therefore, the developed photo-crosslinkable PCLs were evaluated as starting materials in digital light processing (DLP). DLP

is a projection-based 3D-printing technique that exploits a digital mirror device (DMD) to create objects in a layer-by-layer fashion. As a result, the manufacturing time scales linearly with the intended volume. Therefore, the manufacturing speed and cost-efficiency of this technique is considerably enhanced compared to conventional extrusion-based 3D-printing.[48] Furthermore, the resolution of DLP generally ranges between 25 – 150 µm, while the resolution for extrusion-based 3D-printing generally ranges between 100 – 600 µm.[49] Thus, in addition to the increased manufacturing speed, the resolution is also superior compared to extrusion-based 3D-printing. Finally, it should be noted that, based on the gelation point (i.e. crossover of G' and G'') of the thiol-yne photo-crosslinked PCL (717 seconds, Figure 5), this materials was not considered for DLP.

DLP processability depends on multiple factors, including the viscosity of the resin, the penetration depth of the curing light and the minimal energy required for polymerization.[50] First, a suitable solvent and concentration was selected. To do so, the solubility of the developed PCLs, the boiling point of the solvents and the viscosity of the resulting solutions were taken into account. On the one hand, the boiling point of the solvent should be high enough to prevent evaporation during printing. On the other hand, the boiling point of the solvent should be low enough to be effectively removed post-printing. This is important to avoid toxicity issues that are often concomitant with the use of organic solvents. Based on this, a concentration of 60 w/w % of the respective PCLs in toluene was considered optimal as this resulted in a viscosity of 0.6 Pa.s at room temperature (Figure S7). This viscosity is well below 10 Pa.s, generally referred to as the maximal viscosity threshold compatible with DLP.[51]

Secondly, a range of photo-initiator (PI, 1 – 10 mol.% TPO-L) and photo-absorber (PA, 1:200 – 1:500 ratio of PI:PA) concentrations were evaluated. As photo-absorber, Quinoline Yellow (QY) was selected due to its excellent biocompatibility (i.e. allowed in food applications – E104), solubility in toluene and strong absorption at 405 nm. In order to evaluate the different formulations, a CAD design with cubes (sides of 1 000, 500, 250 and 100 µm) that decreased

in size was created (Figure S8). The height of the cubes was 0.5 mm (10 layers of 50 µm thick). Then, based on an iterative approach by variation of the intensity (7- 30 mW/cm²) and the irradiation time (1-5 seconds), the X-Y resolution of the formulations was macroscopically assessed. Ultimately, a formulation that contained 10 mol.% TPO-L (according to crosslinkable functionalities) and 0.01 wt.% QY was found to result in macroscopically well-defined cubes utilizing an intensity of 27.8 mW/cm² and an irradiation time of 3.5 seconds. This was further confirmed via evaluation of the printed objects via optical microscopy. Indeed, as shown in Figure 7A, the developed formulations resulted in an excellent agreement between the experimental and theoretical dimensions for all feature sizes, with the highest deviation occurring for the 100 µm features being 12 µm (Table S1). Thus, the X-Y resolutions achieved here correspond well with earlier reports in literature for biomaterials.[49]

Next, the penetration depth of the curing light (D_p) and the minimal energy required for polymerization (E_c) of the different formulations was elucidated. In order to do so, the respective working curves were determined. The working curve was firstly reported by Jacobs and describes the relation between the applied dose (E) and cured thickness (C_d) of the resin (Equation 1).[52]

$$C_d = D_p \ln\frac{E}{E_c} \quad (1)$$

An established procedure based on confocal microscopy to determine the cured thickness was exploited as it is reported to be more accurate compared to the use of a caliper (Figure S9).[50] The obtained working curves are shown in Figure 7B. By fitting of the respective working curve and extrapolation, the penetration depth of the curing light (D_p) and the minimal energy required for polymerization (E_c) could be identified. The R^2 values (corresponding to the linear fits) differed less than 0.01 from 1 illustrating excellent linear fits. As can be seen, critical doses (E_c) of 30.6, 33.8 and 80.3 mJ/cm² were determined for the acrylate, acrylate-thiol and thiol-ene photo-crosslinked PCL, respectively (Figure 7B). Interestingly, higher irradiation doses are

needed to reach the polymerization threshold in case of the thiol-ene photo-crosslinked PCL. This corresponds well with the obtained photo-rheology results described earlier (*vide supra*). However, it should be noted that photo-rheology was performed using a broadband UVA-light source while the DLP was equipped with a 405 LED light source. Therefore, correlations made between photo-rheology and the determined working curves should be approached with caution. Finally, penetration depths (D_p) of 212, 300 and 276 µm were determined for the acrylate, acrylate-thiol and thiol-ene photo-crosslinked PCL (Figure 7B).

Next, it was evaluated whether the same pronounced effect of the photo-crosslinking chemistry on the mechanical properties would be observed in case of DLP-printed dogbones. To do so, tensile testing was again performed, now using dogbones that were DLP-printed using the respective formulations (Figure S10). The printed dogbones had a thickness of 0.5 mm (10 layers of 50 µm). Evaluation of the DLP-printed dogbones illustrated a similar, unprecedented effect of the photo-crosslinking chemistry on the constructs' mechanical properties (Table 4, Figure 7C). Incorporation of PETA-4SH into the acrylate photo-crosslinked network resulted in a 2-fold, 6-fold and 2-fold increase in the Young's modulus, elongation at break and ultimate strength, respectively. The 3D-printed samples thus showed a comparable trend as observed previously (*vide supra*). Interestingly, the obtained values for the Young's modulus, elongation at break and ultimate strength for the acrylate (AUP-PCL) and acrylate-thiol (AUP-PCL + PETA-4SH) photo-crosslinked PCLs are reduced by a factor 2 when compared to the previously obtained values. The latter is due to the reduced polymer concentration that was used in case of DLP-printing because of viscosity restrictions (compared to photo-crosslinking from melt). In case of the 3D-printed thiol-ene photo-crosslinked PCL, this effect was also observed. However, the Young's modulus was reduced from 93.4 ± 5.3 to 1.2 ± 0.1 MPa. It is hypothesized that this decrease results from a loss of crystallinity, as the obtained Young's modulus corresponds well with values obtained for non-crystalline samples (*vide supra*). This might be attributed to solvent traces still being present. However, in order to fully elucidate why this formulation

resulted in a loss of crystallinity, further research is necessary. The elongation at break, on the other hand, increased even further from 736 ± 47 to 1203.3 ± 76.4 % for DLP-printed dogbones. Interestingly, if the stress was relieved at an elongation of 1000 %, the printed dogbones fully returned to their initial length. This indicates that non-crystalline, thiol-ene photo-crosslinked PCL results in very elastic networks. Moreover, the elasticity is amongst the highest values ever reported for chemically crosslinked biomaterials (i.e. rubber).[53]

To further illustrate the suitability of the developed materials for tissue engineering, the possibility to print more complex and porous designs was also evaluated. Indeed, for tissue engineering, the development of porous scaffolds is crucial as an interconnected porous structure can enable cell ingrowth and vascularization.[6] As a proof of concent, the thiol-ene photo-crosslinked PCL was selected due to its unprecedented mechanical properties. A light dose of 97.3 mJ/cm² proved to be effective to obtain porous structures. This corresponds well with the critical dose (C_d) of 80 mJ/cm² determined via the working curve. It should be noted that the effective dose should slightly exceed the critical dose to ensure proper adhesion between subsequent layers.[54] First, a small boat (± 0.5 cm³) with a window (± 2 mm²) was printed (Figure 7E_{II}). Furthermore, a gyroid scaffold (± 4 cm³) was printed which is a model that is often used in tissue engineering to mimic the structure of cancellous bone (Figure 7E_I). Moreover, porous scaffolds based on 90 ° alternating struts were printed with different pore sizes (250 and 500 µm) (Figure 7D_{III}). Finally, via optical microscopy it was illustrated that uniform pores of 250 µm could be obtained for the design based on 90 ° alternating struts (Figure 7E). To conclude, these preliminary results illustrate that the developed photo-crosslinked PCLs can be effectively used to print porous structures. Overall, this further highlights the potential of the developed thiol-ene photo-crosslinked PCL for biomedical applications where extremely elastic or tough photo-crosslinked PCL networks are required (i.e. minimally invasive surgery or tissue engineering).

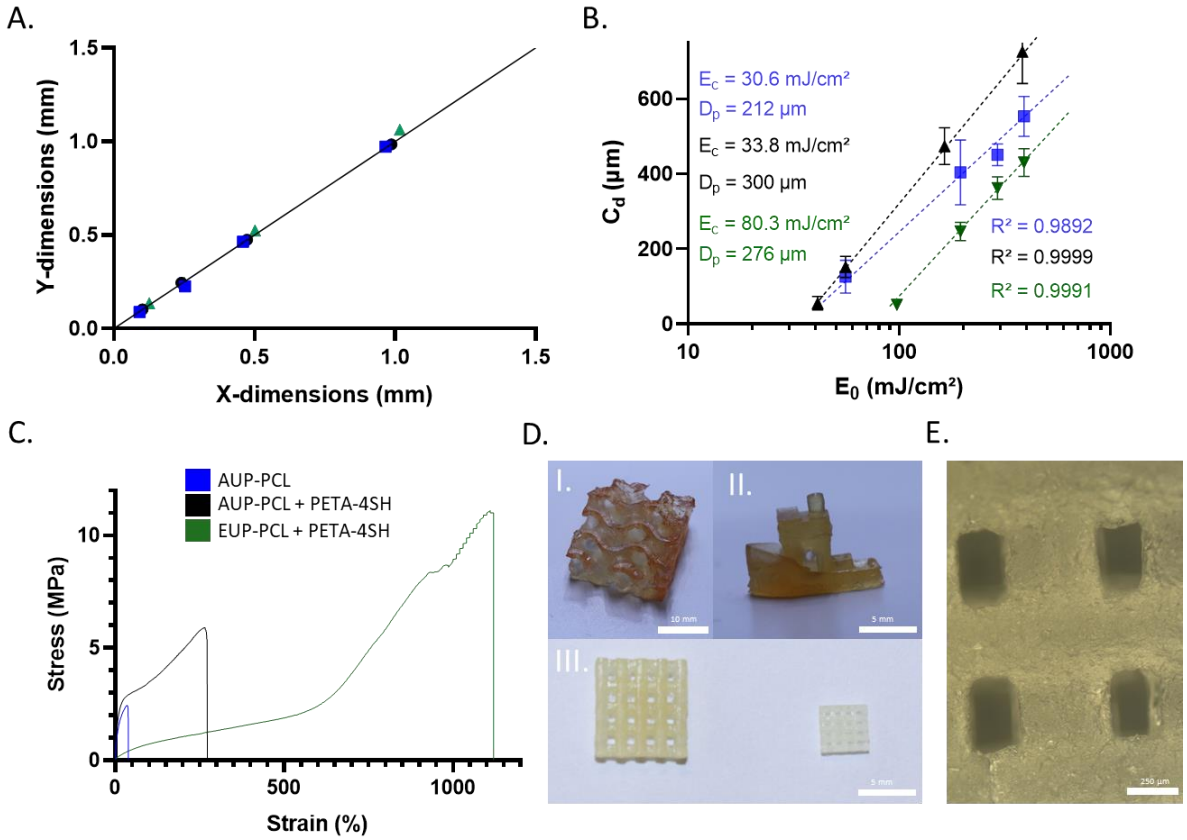

Figure 7. A. Theoretically (black line) and experimentally determined feature sizes for DLP-printed cubes (sides of 100, 250, 500 and 1000 µm); B. Working curves of the DLP-formulations exposed to 405 nm (27.8 mW/cm²). E_c represents critical curing dose, D_p polymerization depth. R^2 values deviate less than 0.01 from 1 illustrating good linear fits; C. Stress-strain curves obtained via tensile testing of DLP-printed dogbones; D. Images of DLP-printed gyroid structure (I.), boat (II.) and porous scaffolds (III) using a resin based on EUP-PCL + PETA-4SH; E. Optical microscopy image of porous scaffold (D_{III}) illustrating well defined pore sizes.

Table 4. Young's moduli, elongations at break, ultimate strengths and toughness's obtained via tensile testing of the photo-crosslinked networks.

#	Young's modulus (MPa)	Elongation at break (%)	Ultimate strength (MPa)
AUP-PCL	19.9 ± 2.7	41.2 ± 11.6	3.0 ± 0.5
AUP-PCL + PETA-4SH	28.2 ± 3.0	237.3 ± 115.2	7.1 ± 2.1
EUP-PCL + PETA-4SH	1.2 ± 0.1	1203.3 ± 76.4	12.0 ± 2.1

[a)] reported values are the average of triplicates ± standard deviation.

3. Conclusions and future perspectives

In summary, the network topology has been introduced as a strategy to optimize the mechanical properties of photo-crosslinkable bioresorbable PCL networks. Photo-crosslinked PCL

networks resulting from acrylate, acrylate-thiol, thiol-ene and thiol-yne photo-crosslinking were synthesized, characterized and their *in vitro* biocompatibility was evaluated. Controlling the network topology proved to be an efficient method to greatly enhance the elasticity and toughness of photo-crosslinked PCL networks. Furthermore, indirect and direct cytotoxicity testing has shown these materials to be non-cytotoxic. Moreover, osteogenic differentiation of ADSCs was illustrated by the presence of Ca^{2+}-deposits after 14 days of cell culture on gelatin-coated samples. Finally, their applicability in digital light processing, a light-based 3D-printing technique was successfully illustrated. As a result of the superior mechanical properties, non-cytotoxicity and excellent DLP-printability, the herein reported photo-crosslinked PCL networks have the potential to pave the way towards the application of light-based additive manufacturing exploiting biodegradable polyesters as starting materials for tissue engineering purposes.

4. Experimental Section

Materials: Poly-ε-caprolactone diol (M_n = 2000 g.mol^{-1}, Sigma Aldrich), chloroform (> 99.5%, Chem-LAB), isophoronediisocyanate (IPDI, 98%, Sigma Aldrich), ethyl (2,4,6-trimethylbenzoyl) phenylphosphinate (TPO-L speedcure), 1-methyl-2-pyrrolidone (NMP, 99%, Sigma Aldrich), dimethyl terephthalate (DMT, TraceCERT, Sigma Aldrich), HCL (1N in isopropanol, Fischer Sci), pentaerythritol tetrakis(3-mercaptopropionate) (PETA-4SH, > 95%, Sigma Aldrich), 2-hydroxyethyl acrylate (96%, Sigma Aldrich), dibutylamine (99.5 %, Sigma Aldrich), allyl alcohol (> 99%, Sigma Aldrich), propargyl alcohol (> 99%, Sigma Aldrich) were used as received. Poly(ε-caprolactone) (70 000 – 90 000 g.mol^{-1}, Sigma Aldrich). Bismuth neodecanoate and phenothiazine (PTZ) were provided by Allnex (Belgium). Toluene (> 99.9%, Chem-lab) was refluxed over sodium with benzophenone as indicator and distilled before use.

Synthesis of the functionalized PCLs: IPDI (2 eq., M = 222.28 g.mol^{-1}) was weighed in a flame-dried two-neck flask under argon atmosphere. PTZ (M = 199.27 g.mol^{-1}, 15 mg, 0.075 mmol) and bismuth-neodecanoate (M = 722.75 g.mol^{-1}, 15 mg, 0.021 mmol) were added as inhibitor

and catalyst respectively. Subsequently, the mixture was heated to 60 °C followed by dropwise addition of 2-hydroxyethyl acrylate (2 eq., M = 116.12 g.mol^{-1}), allyl alcohol (2 eq., M = 58.08 g.mol^{-1}) or propargyl alcohol (2 eq., M = 56.06 g.mol^{-1}) for the synthesis of AUP-PCL, EUP-PCL and YUP-PCL, respectively. After addition, the mixture was left to stir for 1 hour. Isocyanate quantification (*vide infra*) using dibutylamine indicated that the reaction was finished. The IPDI adduct was subsequently cooled in an ice-bath and directly used in the following step without further purification. In the second step, PCL diol (1 eq., M = 2000 g.mol^{-1}, 20.000 g, 10 mmol) was dissolved in toluene in a flame-dried two-neck flask equipped with a stirring bar. To the solution, PTZ (M = 199.27 g.mol^{-1}, 15 mg, 0.075 mmol) and Bismuth neodecanoate (M = 722.75 g.mol^{-1}, 15 mg, 0.021 mmol) were added after which the mixture was heated to 60 °C. Subsequently, the IPDI adduct prepared in the previous step was added dropwise to the solution. After addition, the reaction temperature was increased to 80 °C and the mixture was left to react overnight. Via FTIR spectroscopy, complete conversion of the isocyanates could be confirmed through the disappearance of the isocyanate stretching vibration at 2275-2250 cm^{-1}. Finally, AUP-PCL, EUP-PCL and YUP-PCL were purified via precipitation in cold diethyl ether with a yield of 64 %, 63 % and 70 %, respectively.

Determination of the degree of substitution: The degree of substitution was determined via quantification of the acrylate, alkene and alkyne functionalities, herein referred to as the functional content (mol.g^{-1}). In order to do so, ^{1}H-NMR samples were prepared in $CDCl_3$ containing the respective PCL-derivatives and dimethyl terephthalate (DMT) was used as internal standard. Subsequently, the double bond content was calculated using the following formula:

$$Functional\ content\ (mol.g^{-1}) = \frac{(characteristic\ peaks)}{I_8} \times \frac{n_{double}}{n_{DMT}} \times \frac{m_{DMT}}{M_{DMT}} \times \frac{1}{m_{PCL}} \qquad (2)$$

In this equation, n_{double} and n_{DMT} refer to the number of protons of the integrated signals corresponding to the acrylate/alkene/alkynes and DMT (I_8), m_{DMT} and M_{DMT} refer to the mass

and the molar mass of DMT, m_{PCL} refers to the mass of the modified PCL. I_8 refers to the intensity for the peak at a shift of 8 ppm which corresponds to the aromatic protons of DMT (n = 4). Finally, the characteristic peaks employed for the different modified PCLs are the following: AUP-PCL ($I_{6.40}$, $I_{6.12}$ and $I_{5.83}$), EUP-PCL ($I_{5.9}$, $I_{5.2}$ and $I_{5;3}$) and YUP-PCL ($I_{4.27}$). The obtained double bond molar concentration was then used to calculate the degrees of substitution according to the theoretical molar mass of the final products (AUP-PCL = 84%, EUP-PCL = 73% and YUP-PCL = 82%). Further information is provided in the supplementary information.

Isocyanate quantification: The isocyanate content was determined via back-titration with dibutylamine using an automatic titrator equipped with 1 M HCl. First, a solution containing 64.5 g dibutylamine (64.5 g, 0.499 mol) in 1L NMP was prepared. Approximately 200 mg of the reaction mixture was reacted with 3 mL of the dibutylamine solution in 50 mL NMP during 15 minutes of stirring. Subsequently, the residual dibutylamine was quantified through automatic titration using HCL (1M in isopropanol). The isocyanate concentration could be calculated using following formula:

$$Isocyanate\ content\ (mmol.g^{-1}) = \frac{(V_{blanc} - V_{sample}) \times C_{HCl}}{m_{sample}} \quad (3)$$

In this equation, V_{blanc} and V_{sample} refer to the employed volume of the blank and the sample respectively, C_{HCL} refers to the concentration of the HCL solution (1M in isopropranol) and m_{sample} refers to the mass of the sample.

Photo-curing: In order to obtain photo-crosslinked films, 4 g of the respective functionalized PCL (AUP-PCL, EUP-PCL and YUP-PCL) was dissolved in $CHCl_3$. Subsequently, TPO-L (2mol.% according to double bonds) as photo-initiator and PETA-4SH (in case of AUP-PCL + PETA-4SH, EUP-PCL + PETA-4SH and YUP-PCL + PETA-4SH) were added to the solution. An acrylate to thiol ratio of 2:1, 1:1 and 1:2 was employed for AUP-PCL + PETA-4SH, EUP-PCL + PETA 4-SH and YUP-PCL + PETA-4SH, respectively. The solution was vigorously

stirred followed by evaporation of $CHCl_3$ under reduced pressure. Finally, the melt was heated to 50 °C and placed in between a glass mold, equipped with a silicone spacer and PTFE release foil. The mold was then exposed to UV-A irradiation (315-400 nm, 10 mW/cm²) at room temperature during 30 minutes (and 2 hours for the thiol-yne photo-crosslinked PCL). It should be noted that photo-crosslinking is significantly faster than the timeline during which crystallization occurs. After photo-crosslinking of the sheets, no crystalline domains are present, thus, the influence of crystallization on the photo-crosslinking process can be considered negligible. The thickness of the sheets post photo-crosslinking was determined to be 50 µm.

Characterization: Structure elucidation was performed through ^{1}H-NMR spectroscopy using a Bruker spectrometer (400 MHz) with $CDCl_3$ as solvent and Fourier-transform infrared spectroscopy (FTIR) using a Perkin-Elmer spectrometer. FTIR spectra were recorded for the range of 700-4000 cm^{-1} with a resolution of 4 cm^{-1} and a data interval of 1 cm^{-1}. HRMAS was obtained using a Bruker spectrometer (700 MHz) with $CDCl_3$ as solvent. The thermal properties were studied by thermogravimetric analysis (TGA – TA instruments Q50) and differential scanning calorimetry (DSC – TA instruments Q2000). The crystallinity was calculated, based on an enthalpy of fusion of 135 J/g.[55] TGA was performed starting from 30 °C up to 600 °C with a heating rate of 10 °C per minute under nitrogen atmosphere. DSC was performed using ~ 5 mg of sample using Tzero aluminum pans sealed with an aluminum Tzero lid. In the first heating cycle, the sample was heated from 30 °C up to 100 °C and subsequently cooled to – 80 °C. Thereafter, the sample was heated again heated to 100 °C, during the second heating cycle. Heating and cooling rates of 10 °C per minute were employed under nitrogen atmosphere. Swelling and gel fraction experiments were performed using 3 mm diameter discs which were punched out from crosslinked films with a thickness of 0.5 mm. The samples were immersed in $CHCl_3$ during 24 hours and subsequently dried under vacuum during 24 hours at 80 °C. Degrees of swelling and gel fractions were calculated using the following formulas:

$$Gel\ fraction = \frac{m_d}{m_i} \times 100\ (\%) \quad (4)$$

$$Degree\ of\ swelling = \frac{m_s - m_d}{m_i} \quad (5)$$

Here m_d refers to the dry mass, m_s to the swollen mass and m_i to the initial mass before swelling. Tensile experiments were performed using a Tinius Olsen Model 1 ST apparatus, equipped with a load cell of 250 N using Horizon as software. An initial strain rate of 1 mm per minute was used up to a force of 0.1 N after which the strain rate was increased to 10 mm per minute. Photo-rheology was performed using an Anton Paar Physica MCR 301 rheometer equipped with a UV light-source (365 nm, 3500 mW/cm²) with a parallel plate set-up (top plate diameter: 25 mm). 300 µL of the polymer melt was placed between the plates with the gap set to 300 nm. The measurements were performed at 20 °C, at a strain rate of 0.1 % and a frequency of 1 Hz. DMA experiments were performed in tension using rectangular samples (9 mm length, 3 mm width and 0.6 mm thickness) with a heating rate of 3 °C/minute from – 80 °C up to 80 °C. To plasma-treat the samples, a Diener Femto (version 5) was used equipped with a 40 kHz generator (100 W). Plasma treatment was applied on both sides during one minute under a stable oxygen pressure of 0.8 mbar. A Zeiss Axiotech 100 HD/DIC light microscope was used together with ZenCore software.

In vitro biological evaluation: 3T3 (Merk, Germany) cells were maintained at 37°C in 5% CO_2 in Dulbecco's Modified Eagle Medium (DMEM, Sigma-Aldrich, UK) supplemented with 10% (v/v) foetal calf serum (InvitrogenTM, UK) and 1% (v/v) penicillin/streptomycin (InvitrogenTM, UK). The culture media was changed every third day. Once cells had reached between 90 and 95% confluency, they were mechanically scraped and sub-cultured under the same conditions.

Human Foreskin fibroblasts (HFF, ATCC) and Adipose-derived Stem Cells (ADSC, Sigma Aldrich) were cultured at 37°C in 5% CO_2 in Dulbecco's Modified Eagle Medium (DMEM, Sigma-Aldrich, BE) supplemented with 10% (v/v) fetal bovine serum (FBS, Sigma-Aldrich,

BE) and 1% (v/v) penicillin/streptomycin (Sigma-Aldrich, BE). The culture media were changed twice a week. Sub-culturing followed after reaching 80-90% confluency. HFF were used at passage number 12 and ASCs at passage number 5.

Photo-cured samples for cell culture were sterilized through incubation in a 70% (v/v) ethanol solution for 24 hours with a refreshment step after 12 hours. Subsequently, UV-C irradiation (100-280 nm, 15 mW/cm^2) was applied.

For the differentiation assay, a gelatin coating was applied according to a previously established procedure. [56] 8 mm discs of the respective material were oxygen-plasma treated on both sides (1 min, 100 W). The samples were subsequently immersed in a gelatin-methacrylamide (GelMA) solution of 1 w/v % in water in the presence of 1 mol.% of Irgacure 2959 (relative to acrylate content). Finally, the discs were taken out of the solution and irradiated using UVA irradiation (10 mW/cm², 1 hour). GelMA was obtained according to a previously reported protocol.[56] 100 g gelatin B was dissolved in 1 L phosphate buffer at 40 °C. Methacrylic anhydride was added (3 eq. relative to the primary amines) and left to react for 1 hour. The reaction was then quenched with 1 L of distilled water. Finally, the purified product was obtained after dialysis and lyophilization. The degree of substitution was determined to be 100 % through ^{1}H-NMR spectroscopy (according to the characteristic signals of Val, Leu and Ile as previously reported).[56]

For the NRU assay, 3T3 cells which were seeded into 96-well plates at a density of 1 x 10^4 cells/well to form a sub confluent monolayer. After 48 h, the culture medium was removed, and three different dilutions (100 % extract, 50 % extract, and 25 % extract) of the test compounds in medium were added to the cells and incubated for 24 h at 37 °C in 5 % CO_2. Treatment medium was used as the untreated vehicle control. After treatment with the extracts, cells were washed once with PBS, and treated with Neutral Red dye for 3 h at RT, followed by NR desorb (ETOH/acetic acid) solution added to all wells. The absorption of the resulting coloured solution was measured at 540 nm in a plate reader. Cell viability was calculated as the

percentage of vehicle control (cell culture media only) values. For the treatment extracts, all compounds were extracted at a ratio of 3 cm^2 / ml in vehicle medium for 72 h before being added to cell culture.

A direct contact biocompatibility assay was initiated through seeding of 10000 HFF into the wells of a 96-well plate. After one day, the sterilized samples were placed on top of the cultured monolayer. Seven days later, the viability and metabolic activity of the monolayer was investigated through a Live/Dead (Calcein-acetoxymethyl (Sigma-Aldrich, BE) /Propidium iodide (PI, Sigma-Aldrich, BE)) and a 3-(4,5-dimethylthiazol-2-yl)-5-(3-carboxymethoxyphenyl)-2-(4-sulfophenyl)-^{2}H-tetrazolium (MTS, Abcam, NE) assay respectively. First, the photo-crosslinked samples were removed and the culture medium was discarded.

Thereafter, in order to quantify the cell viability, a 2 % (v/v) CA-AM/PI in phosphate buffered saline (PBS) solution was added to the monolayer of cells and incubated in the dark at room temperature for 10 minutes. The cells were visualized through a green fluorescent protein (GFP) and a Texas Red (TxRed) filter of a fluorescence microscope (Olympus IX81 with Xcellence Pro software). The percentage viability was computed through the use of FIJI software.

Furthermore, in order to quantify the cell metabolic activity, a 17 % (v/v) solution of MTS in culture medium was added to the monolayer of cells and incubated in the dark at 37 °C for 2 hours under continuous shaking. The absorbance was then quantified at 490 nm with a spectrophotometer (BioTek Instruments, EL800 Universal Microplate Reader, with GEN5 software).

For the osteogenic differentiation experiment, 10000 ASC / cm^2 were seeded on top of the sterilized and coated samples. After 1 day, the medium was discarded and refreshed with osteogenic medium (culture medium supplemented with 100 nM dexamethasone (Sigma-Aldrich, BE), 10 mM β-glycerolphosphate (Sigma-Aldrich, BE) and 0.08 mM ascorbic acid (Sigma-Aldrich, BE)). Two weeks after the osteogenic medium induction, the samples were

stained with Alizarin red (Sigma-Aldrich, BE) to visualize the deposition of calcium as a marker of osteogenesis.

To this end, the medium was discarded and the samples were washed twice with PBS. 4 % (w/v) paraformaldehyde (Sigma-Aldrich, BE) fixative was added for 10 minutes followed by washing twice with PBS and once with distilled water. Thereafter, the samples were incubated with a 1 % (w/v) Alizarin red solution for 20 minutes at room temperature with gentle shaking. The wells were then washed with excess distilled water until the background staining was maximally cleared. Calcium deposits were visualized with an optical microscope (Zeiss Axiotech 100 HD with ZenCore software). Furthermore, the calcium was extracted through addition of 10 % (v/v) acetic acid to each well followed by incubation for 30 minutes at room temperature while shaking. Standards were made through serial dilutions of the 1 % (w/v) Alizarin red staining solution (1 in 10, 1 in 50, 1 in 100, 1 in 500, 1 in 1000, 1 in 10 000 and 0). Both standards and samples were brought to a pH of 4.1 whereafter the absorbance was quantified at 405 nm with a spectrophotometer (BioTek Instruments, EL800 Universal Microplate Reader, with GEN5 software).

Digital light processing (DLP): A LumenX DLP-printer from Cellink was used. This device is equipped with a 405 nm light emitting diode (LED) and a digital mirror device (DMD). The build platform offset was set to 0 and no heating was applied during printing. During printing of the cubic constructs, an intensity of 70 % was used (27.8 mW/cm²). This was determined before each printing session by means of a dosimeter. All formulations contained 60 w/w% of the respective photo-crosslinkable PCL in toluene, 10 mol.% TPO-L as photo-initiator (with respect to the terminal groups) and 1:300 molar ratio of quinoline yellow as photo-absorber. PETA-4SH was added according to a 2:1 and 1:1 ratio in case of acrylate-thiol and thiol-ene photo-crosslinked PCL, respectively. Each layer was illuminated for 3.5 seconds and a first layer factor of 2 was used. The CAD design is shown in Figure S8 and the height was 0.5 mm (10 layers of 50 µm thick). Post-processing of the printed objects included thoroughly washing

with acetone and subsequent post-curing through UVA irradiation (10 mW/cm², 10 minutes). The working curves were obtained by measuring the thickness of a cured layer for different cure doses. To do so, squares of 1 cm² were printed on glass slides using 70 % intensity (27.8 mW/cm²) and increasing irradiation times (2-14 seconds). No build platform was used as this would limit the light penetration in the Z-direction. The cure depths were determined by placing the glass slides horizontally and subsequent measuring of the thickness using a light-microscope (Zeiss Axiotech). For each applied dose, three different samples were measured, at three different locations. To illustrate this, optical microscopy images of photo-cured layers upon increasing doses are included in the supporting information (Figure S9). In order to DLP-print the dogbones, identical settings as previously described were used. The CAD design as well as a picture of the 3D-printed dogbones is shown in Figure S10. Tensile testing of the DLP-printed dogbones was performed using a Tinius Olsen Model 1 ST apparatus, equipped with a load cell of 250 N using Horizon as software. An initial strain rate of 1 mm per minute was used up to a force of 0.1 N after which the strain rate was increased to 10 mm per minute. Finally, identical parameters as described before were used to print the more complex and porous objects using thiol-ene photo-crosslinked PCL. However, additional sonication of the printed structures in the presence of acetone was necessary to remove uncured resin from the pores.

Supporting Information
Supporting Information is available from the Wiley Online Library or from the author.

Acknowledgements

The authors would like to acknowledge funding from FWO (FWO-SB fellow - 1SA2321N) and Interreg 2Seas 3DMed. Furthermore, the authors would like to acknowledge Bernhard De Meyer for the DMA analysis. The 700 MHz used in this work is part of the NMR Expertise Centre at UGent and was funded through an FFEU-ZWAP grant awarded to Prof. J. Martins (UGent).

Received: ((will be filled in by the editorial staff))
Revised: ((will be filled in by the editorial staff))
Published online: ((will be filled in by the editorial staff))

References

[1] Z. Sheikh, S. Najeeb, Z. Khurshid, V. Verma, H. Rashid, M. Glogauer, *Materials (Basel).* **2015**, *8*, 5744.

[2] D. Ozdil, H. M. Aydin, *J. Chem. Technol. Biotechnol.* **2014**, *89*, 1793.

[3] G. Thrivikraman, A. Athirasala, C. Twohig, S. K. Boda, L. E. Bertassoni, *Dent. Clin. North Am.* **2017**, *61*, 835.

[4] P. A. Gunatillake, R. Adhikari, N. Gadegaard, *Eur. Cells Mater.* **2003**, *5*, 1.

[5] H. E. Jazayeri, M. Tahriri, M. Razavi, K. Khoshroo, F. Fahimipour, E. Dashtimoghadam, L. E. Almeida, L. Tayebi, *Mater. Sci. Eng. C* **2017**, *70*, 913.

[6] M. Maroulakos, G. Kamperos, L. Tayebi, D. Halazonetis, Y. Ren, *J. Dent.* **2019**, *80*, 1.

[7] P. Tack, J. Victor, P. Gemmel, L. Annemans, *Biomed. Eng. Online* **2016**, *15*, 1.

[8] N. Martelli, C. Serrano, H. Van Den Brink, J. Pineau, P. Prognon, I. Borget, S. El Batti, *Surg. (United States)* **2016**, *159*, 1485.

[9] C. Yu, J. Schimelman, P. Wang, K. L. Miller, X. Ma, S. You, J. Guan, B. Sun, W. Zhu, S. Chen, *Chem. Rev.* **2020**.

[10] A. J. Guerra, H. Lara-Padilla, M. L. Becker, C. A. Rodriguez, D. Dean, *Curr. Drug Targets* **2019**, *20*, 823.

[11] A. Bagheri, J. Jin, *ACS Appl. Polym. Mater.* **2019**, *1*, 593.

[12] M. A. Woodruff, D. W. Hutmacher, *Prog. Polym. Sci.* **2010**, *35*, 1217.

[13] F. J. Van Natta, J. W. Hill, W. H. Carothers, *J. Am. Chem. Soc.* **1934**, *56*, 455.

[14] H. Sun, L. Mei, C. Song, X. Cui, P. Wang, *Biomaterials* **2006**, *27*, 1735.

[15] C. X. F. F. Lam, M. M. Savalani, S. H. Teoh, D. W. Hutmacher, *Biomed. Mater.* **2008**, *3*.

[16] Y. Ramot, M. Haim-Zada, A. J. Domb, A. Nyska, *Adv. Drug Deliv. Rev.* **2016**, *107*, 153.

[17] A. Kumari, S. K. Yadav, S. C. Yadav, *Colloids Surfaces B Biointerfaces* **2010**, *75*, 1.

[18] B. D. Ulery, L. S. Nair, C. T. Laurencin, *J. Polym. Sci. Part B Polym. Phys.* **2011**, *49*, 832.

[19] P. Yang, G. Zhu, S. Xu, X. Zhang, X. Shen, X. Cui, Y. Gao, J. Nie, *J. Polym. Sci. Part B Polym. Phys.* **2017**, *55*, 692.

[20] G. Tian, G. Zhu, T. Ren, Y. X. Liu, K. Wei, Y. X. Liu, *J. Appl. Polym. Sci.* **2019**, *136*, 1.

[21] M. Baker, R. Wang, F. Damanik, T. Kuhnt, H. Ippel, P. Dijkstra, T. Cate, A. Dias, L. Moroni, **2020**.

[22] L. Jiang, J. Zhang, *Biodegradable Polymers and Polymer Blends*, Elsevier, **2013**.

[23] L. Cai, S. Wang, *Polymer (Guildf).* **2010**, *51*, 164.

[24] J. L. E. Ivirico, M. S. Sánchez, R. Sabater i Serra, J. M. M. Dueñas, J. L. G. Ribelles, M. M. Pradas, *Macromol. Chem. Phys.* **2006**, *207*, 2195.

[25] L. Cai, C. J. Foster, X. Liu, S. Wang, *Polymer (Guildf).* **2014**, *55*, 3836.

[26] B. G. Amsden, G. Misra, F. Gu, H. M. Younes, *Biomacromolecules* **2004**, *5*, 2479.

[27] N. B. Cramer, C. N. Bowman, *J. Polym. Sci. Part A Polym. Chem.* **2001**, *39*, 3311.

[28] S. K. Reddy, N. B. Cramer, C. N. Bowman, *Macromolecules* **2006**, *39*, 3681.

[29] N. B. Cramer, S. K. Reddy, M. Cole, C. Hoyle, C. N. Bowman, *J. Polym. Sci. Part A Polym. Chem.* **2004**, *42*, 5817.

[30] C. E. Hoyle, T. A. I. Y. Lee, T. Roper, *J. Polym. Sci. Part A Polym. Chem.* **2004**, *42*, 5301.

[31] T. O. Machado, C. Sayer, P. H. H. H. Araujo, *Eur. Polym. J.* **2017**, *86*, 200.

[32] C. E. Hoyle, C. N. Bowman, *Angew. Chemie - Int. Ed.* **2010**, *49*, 1540.

[33] A. K. O'Brien, N. B. Cramer, C. N. Bowman, *J. Polym. Sci. Part A Polym. Chem.* **2006**, *44*, 2007.

[34] N. B. Cramer, C. N. Bowman, **2017**, *2011*, 117.

[35] Y. Gu, J. Zhao, J. A. Johnson, *Trends Chem.* **2019**, *1*, 318.

[36] F. Di Lorenzo, S. Seiffert, *Polym. Chem.* **2015**, *6*, 5515.

[37] A. F. Senyurt, H. Wei, B. Phillips, M. Cole, S. Nazarenko, C. E. Hoyle, S. G. Piland, T. E. Gould, *Macromolecules* **2006**, *39*, 6315.

[38] E. Yoshii, *J. Biomed. Mater. Res.* **1997**, *37*, 517.

[39] B. H. Northrop, R. N. Co, *J. Am. Chem. Soc.* **2012**, 13804.

[40] J. W. Chan, H. Wei, H. Zhou, C. E. Hoyle, *Eur. Polym. J.* **2009**, *45*, 2717.

[41] R. J. Kowalski, L. A. Ferrara, E. C. Benzel, *Neurosurg. Focus* **2001**, *10*.

[42] A. Banerjee, M. Arha, S. Choudhary, R. S. Ashton, S. R. Bhatia, D. V. Schaffer, R. S. Kane, *Biomaterials* **2009**, *30*, 4695.

[43] G. Tian, G. Zhu, S. Xu, T. Ren, *J. Solid State Chem.* **2019**, *272*, 78.

[44] A. Houben, N. Pien, X. Lu, F. Bisi, J. Van Hoorick, M. N. Boone, P. Roose, H. Van den Bergen, D. Bontinck, T. Bowden, P. Dubruel, S. Van Vlierberghe, *Macromol. Biosci.* **2016**, *16*, 1883.

[45] G. F. Caetano, P. J. Bártolo, M. Domingos, C. C. Oliveira, M. N. Leite, M. A. C. Frade, *Procedia Eng.* **2015**, *110*, 59.

[46] R. Xue, Y. Qian, L. Li, G. Yao, L. Yang, Y. Sun, *Stem Cell Res. Ther.* **2017**, *8*, 1.

[47] K. H. Vining, D. J. Mooney, *Nat. Rev. Mol. Cell Biol. 2017 1812* **2017**, *18*, 728.

[48] P. N. Bernal, P. Delrot, D. Loterie, Y. Li, J. Malda, C. Moser, R. Levato, *Adv. Mater.* **2019**, *31*.

[49] M. Lee, R. Rizzo, F. Surman, M. Zenobi-Wong, *Chem. Rev.* **2020**, *120*, 10950.

[50] J. Bennett, *Addit. Manuf.* **2017**, *18*, 203.

[51] T. Kuhnt, F. L. C. Morgan, M. B. Baker, L. Moroni, *Addit. Manuf.* **2021**, *46*, 102102.

[52] P. F. Jacobs, **1992**.

[53] Q. Chen, S. Liang, G. A. Thouas, *Prog. Polym. Sci.* **2013**, *38*, 584.

[54] A. J. Guerra, J. Lammel-Lindemann, A. Katko, A. Kleinfehn, C. A. Rodriguez, L. H. Catalani, M. L. Becker, J. Ciurana, D. Dean, *Acta Biomater.* **2019**, *97*, 154.

[55] M. Nagata, Y. Yamamoto, *J. Polym. Sci. Part A Polym. Chem.* **2009**, *47*, 2422.

[56] A. Houben, N. Pien, X. Lu, F. Bisi, J. Van Hoorick, M. N. Boone, P. Roose, H. Van den Bergen, D. Bontinck, T. Bowden, P. Dubruel, S. Van Vlierberghe, *Macromol. Biosci.* **2016**, *16*, 1883.

Control of the network topology by selection of the appropriate crosslinking chemistry is introduced as a new strategy to fine-tune bioresorbable photo-crosslinked PCL networks. Photo-crosslinked PCL networks obtained via chain growth polymerization, step growth polymerization and a combination thereof are reported and the influence on the mechanical, thermal and biological properties as well as their DLP processability is elucidated.

Q. Thijssen, L. Parmentier, E. Augustyniak, P-A Mouthuy, S. Van Vlierberghe*

From chain growth to step growth polymerization of photo-reactive PCL: the network topology of bioresorbable networks as a tool in tissue engineering

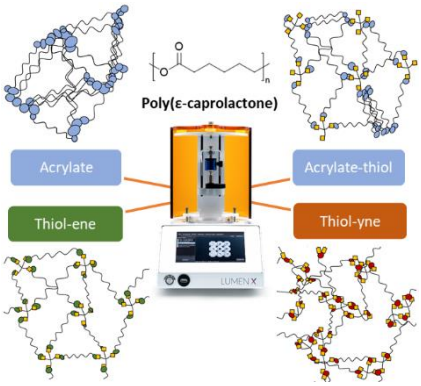

Supporting Information

From chain growth to step growth polymerization of photo-reactive PCL: the network topology of bioresorbable networks as a tool in tissue engineering

*Quinten Thijssen, Laurens Parmentier, Edyta Augustyniak, Pierre-Alexis Mouthuy, Sandra Van Vlierberghe**

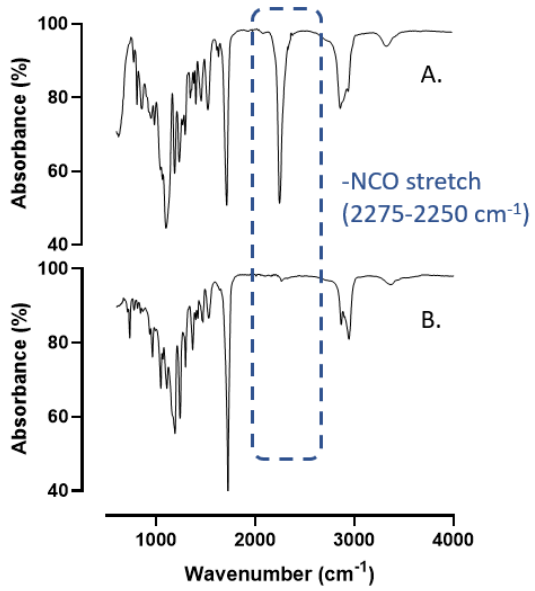

Figure S1. FTIR spectra of A. the intermediate IPDI derivative; B. functionalized PCL indicating the disappearance of the characteristic stretching vibration of the isocyanate functional group after modification.

^{1}H-NMR functional content determination with DMT as internal standard

The degree of substitution (DS) for all materials were determined as the ratio of the experimentally determined concentration of the reactive functionalities in the modified PCL to the theoretical concentration in case of 100 % substitution.

The theoretical concentration in case of 100 % substitution was determined via the molar mass. Therefore, the correct molar mass of PCL diol 2000 was determined via ^{1}H-NMR as 2412 g.mol^{-1} which is further used in the calculations.

It should be noted that the effective DS is most likely higher than the reported values due to the fact that lower molar mass fractions of PCL are more effectively removed via the precipitation, resulting from their higher solubilities in diethyl ether. In order to investigate this, PCL diol 2000 was precipitated which resulted in an increase in molar mass to 2961 g.mol^{-1}.

1. AUP-PCL

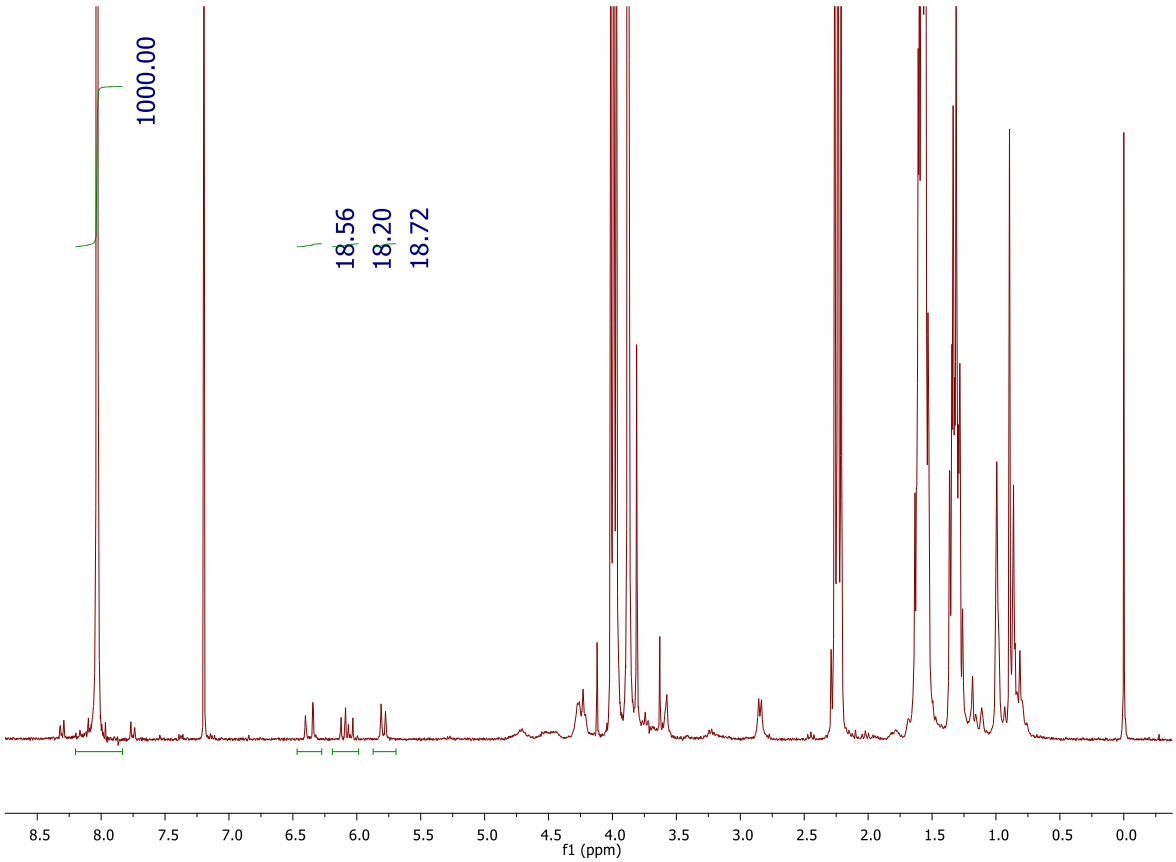

Figure S2. Quantification of the acrylate content of AUP-PCL via ^{1}H-NMR using DMT as an internal standard

M_w(AUP-PCL) = 3089 ➔ 100% substitution ➔ 6.47 . 10^{-4} mol acrylates in one gram AUP-PCL

$$Functional\ content = \frac{18.56 + 18.2 + 18.72}{1000} \times \frac{3}{4} \times \frac{10.2}{194.2} \times \frac{1}{14.6} = 5.45\ .10^{-4}$$

$$Acrylate\ substitution\ degree = \frac{5.45\ .\ 10^{-4}}{6.47\ .\ 10^{-4}} \times\ 100\ \% = 84\ \%$$

2. EUP-PCL

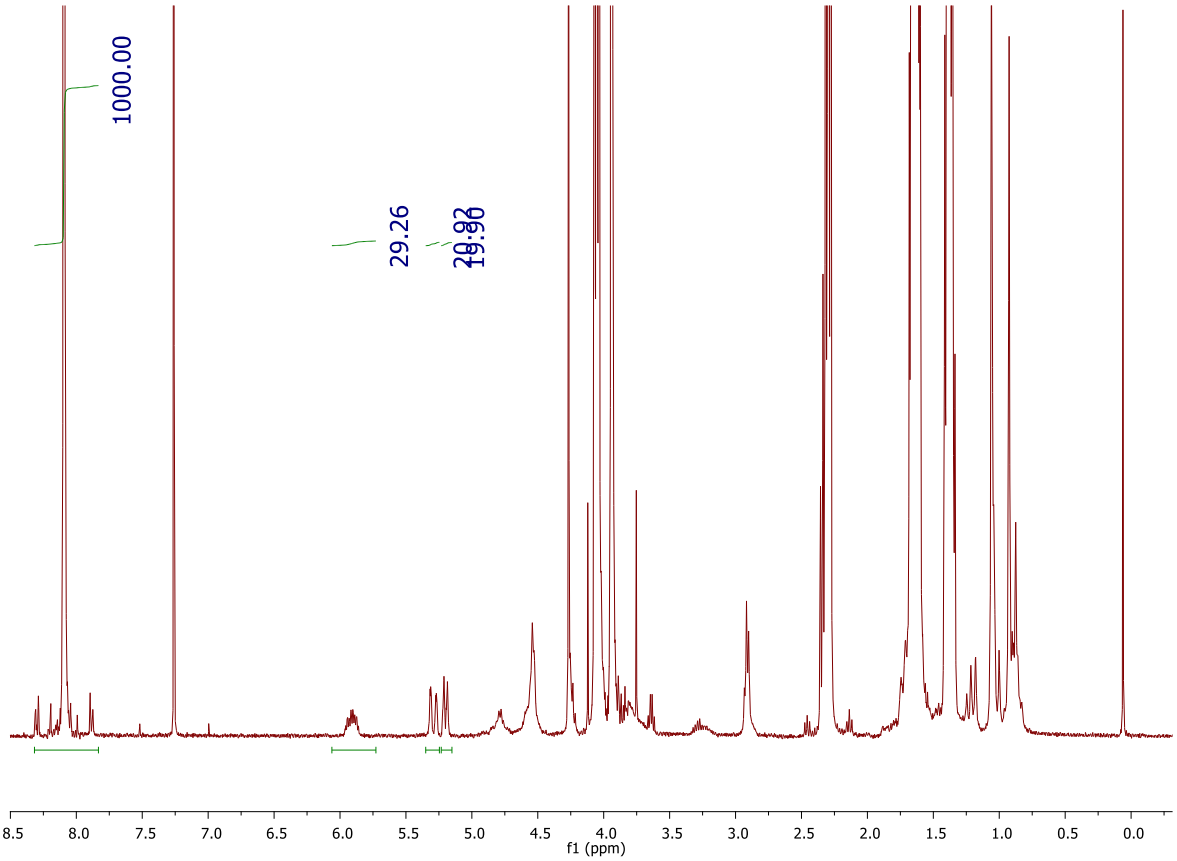

Figure S3. Quantification of the alkene content of EUP-PCL via ^{1}H-NMR using DMT as an internal standard

M_w(EUP-PCL) = 2972 ➔ 100% substitution ➔ 6.73.10^{-4} mol enes in one gram EUP-PCL

$$Functional\ content = \frac{24.51 + 22.94 + 21.61}{1000} \times \frac{3}{4} \times \frac{12.5}{194.2} \times \frac{1}{12.0} = \ 4.94\ .10^{-4}$$

$$Ene\ substitution\ degree = \frac{4.94\ .\ 10^{-4}}{6.73\ .\ 10^{-4}} \times\ 100\ \% = \ 73\ \%$$

3. YUP-PCL

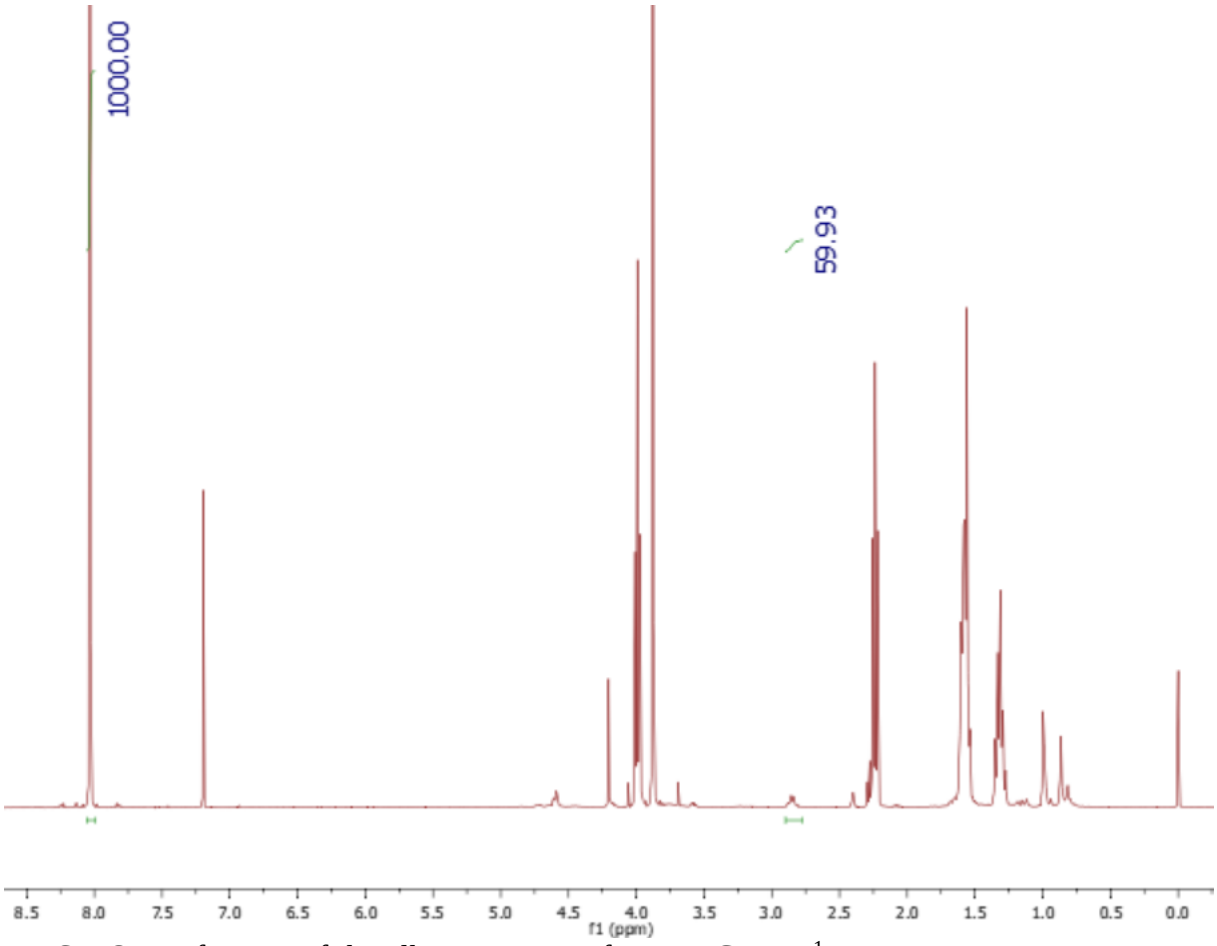

Figure S4. Quantification of the alkyne content of YUP-PCL via ^{1}H-NMR using DMT as an internal standard

M_w(YUP-PCL) = 2968 ➔ 100% substitution ➔ $6.74.10^{-4}$ mol ynes in one gram YUP-PCL

$$Functional\ content = \frac{59.93}{1000} \times \frac{2}{4} \times \frac{9.4}{194.2} \times \frac{1}{10.2} = \ 5.52\ .10^{-4}$$

$$Ene\ substitution\ degree = \frac{5.52\ .\ 10^{-4}}{6.74.\ 10^{-4}} \times\ 100\ \% = 82\ \%$$

Hight resolution magic angle spectroscopy (HRMAS) of the solid crosslinked networks

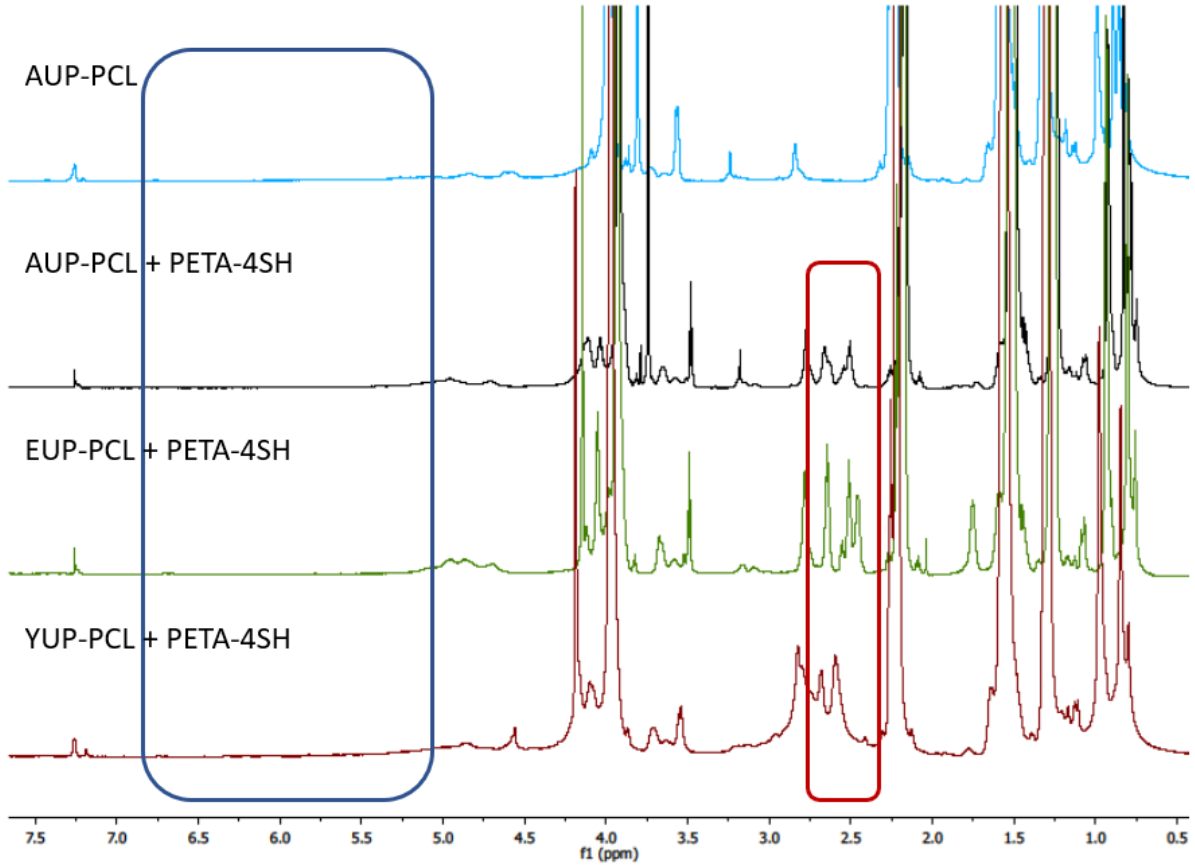

Figure S5. HR-MAS analysis of the solid photo-crosslinked PCL)based networks.
High resolution magic angle spectroscopy (HRMAS) of the solid, crosslinked networks indicating the disappearance of the presence of acrylate/alkenes (alkynes not visible) and thus confirming complete conversion after photo-crosslinking (shown by the blue rectangle). The red rectangle indicates the presence of the peaks corresponding to the structure of PETA-4SH, thereby showing its successful incorporation into the crosslinked networks.

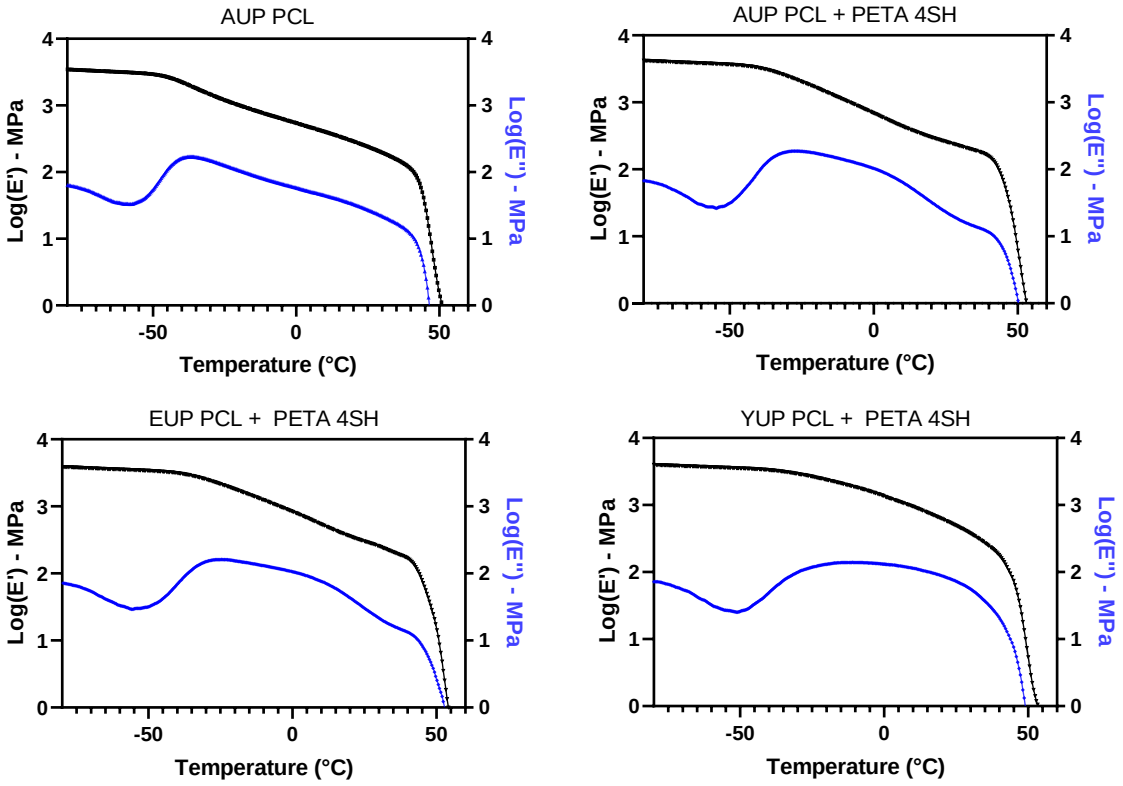

Figure S6. Storage (E') and loss moduli (E'') analyzed by DMA of the PCL-based crosslinked networks with acrylate (AUP-PCL), acrylate-thiol (AUP-PCL + PETA-4SH), thiol-ene (EUP-PCL + PETA-4SH) and thiol-yne crosslinking (YUP-PCL + PETA-4SH).

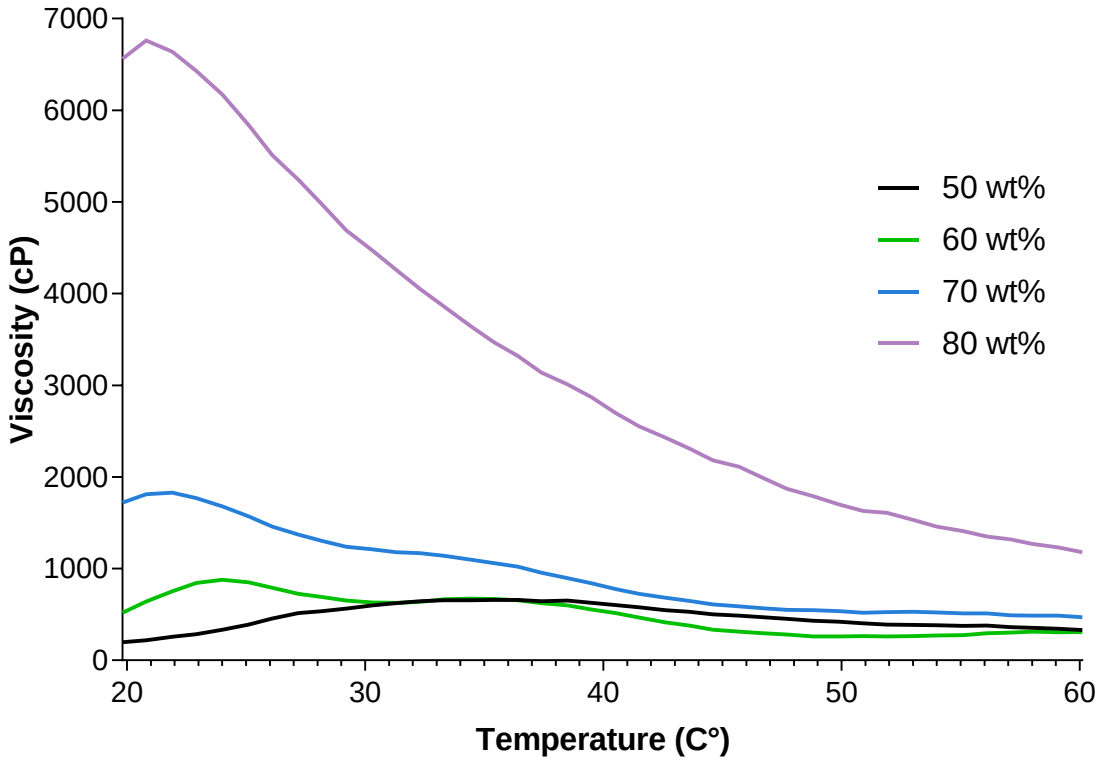

Figure S7. Viscosity in function of temperature of EUP-PCL solutions in toluene with 50 (black), 60 (green), 70 (blue) and 80 (purple) w/w% concentration.

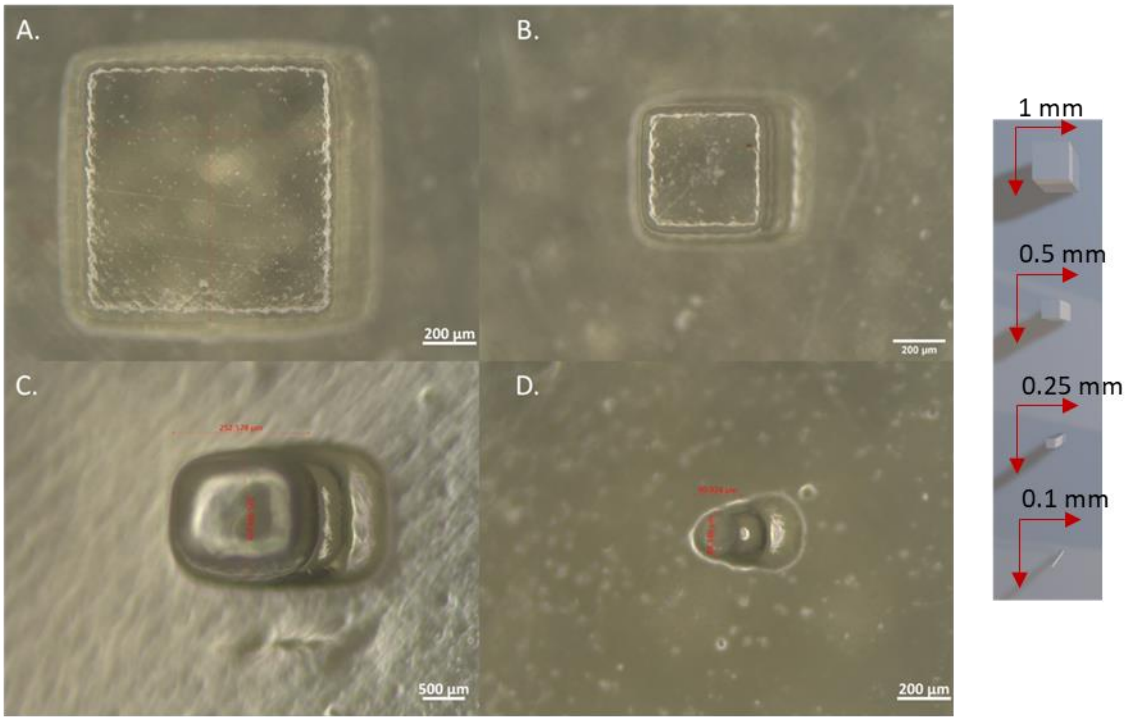

Figure S8. Optical microscopy images illustrating successful 3D-printing of cubic specimens with varying sizes (100, 250, 500 and 1000 µm) using AUP-PCL. The cubic specimens were used to evaluate the resolution of the respective materials for DLP 3D-printing.

Table S1. Theoretical and experimentally determined feature sizes of the DLP-printed cubes of AUP-PCL, AUP-PCL + PETA-4SH and EUP-PCL + PETA-4SH

	Theoretical X & Y dimension (mm)	Experimental X-dimension (mm)	Experimental Y-dimension (mm)
AUP-PCL	0.1	0.091	0.088
	0.25	0.253	0.226
	0.5	0.459	0.464
	1	0.965	0.972
AUP-PCL + PETA-4SH	0.1	0.101	0.102
	0.25	0.24	0.244
	0.5	0.473	0.474
	1	0.986	0.984
EUP-PCL + PETA-4SH	0.1	0.125	0.135
	0.25	0.25	0.244
	0.5	0.501	0.524
	1	1.016	1.063

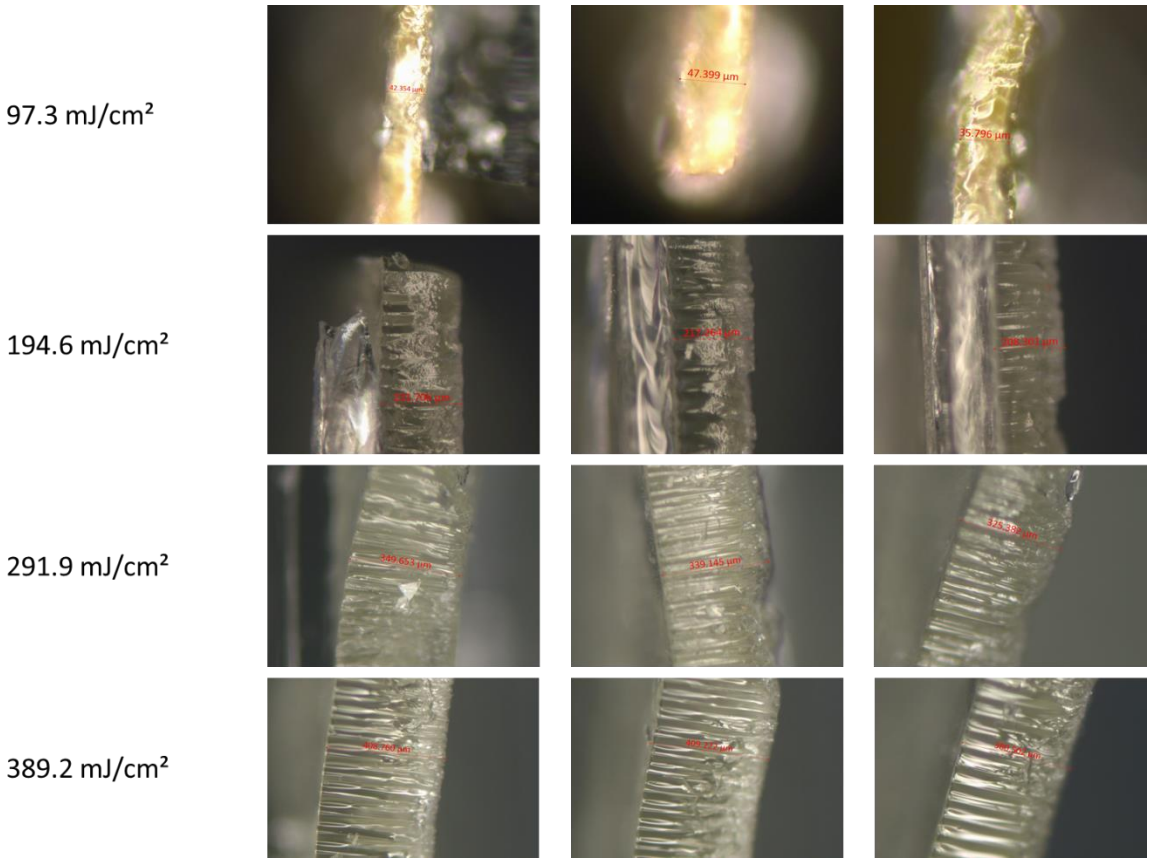

Figure S9. Optical microscopy images to determine the thickness of the photo-cured layers using different curing doses in order to set-up the working curve for thiol-ene photo-crosslinked PCL. All measurements were performed in triplicate and on three different sides of the cured object.

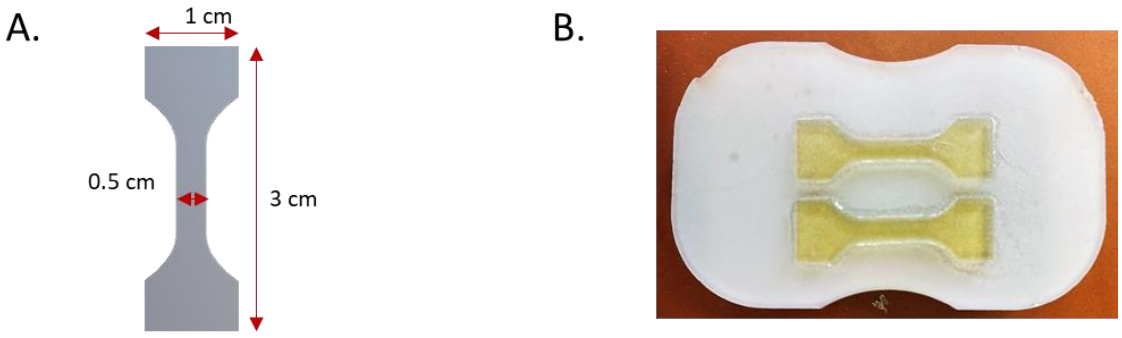

Figure S10. A. Schematic depiction of the CAD model of the dogbones. B. Picture of the DLP-printed dogbones of thiol-ene photo-crosslinked PCL. The DLP-printed dogbones were used in order to evaluate tensile testing properties of the developed materials after 3D-printing. The thickness of the dogbones was 500 µm (10 layers of 50 µm thick).